

# Robust Federated Fine-Tuning in Heterogeneous Networks with Unreliable Connections: An Aggregation View

Yanmeng Wang, *Member, IEEE*, Zhiwen Dai, Shuai Wang, *Member, IEEE*, Jian Zhou, *Member, IEEE*, Fu Xiao, *Senior Member, IEEE*, Tony Q. S. Quek, *Fellow, IEEE*, Tsung-Hui Chang, *Fellow, IEEE*

## Abstract

Federated Fine-Tuning (FFT) has attracted growing interest as it leverages both server- and client-side data to enhance global model generalization while preserving privacy, and significantly reduces the computational burden on edge devices by avoiding training from scratch. Despite these advantages, FFT performance is often degraded by unreliable server-client connections and heterogeneous client data distributions. Most existing methods assume homogeneous network conditions or require prior knowledge of connection failures. However, these assumptions are impractical in real-world networks characterized by diverse communication standards (e.g., wired, Wi-Fi, 4G, and 5G) and heterogeneous failure patterns. To address these limitations, we propose FedAuto, a novel FFT framework that mitigates the combined effects of connection failures and data heterogeneity via adaptive aggregation. FedAuto operates without prior knowledge of network conditions or modifications to existing infrastructure, enabling seamless plug-and-play deployment. Moreover, we establish a rigorous convergence guarantee for FedAuto. By adopting a novel per-round aggregation perspective, our analysis removes the need for assumptions on connection failures probabilities or client selection strategies commonly imposed in prior work, and guarantees convergence of FedAuto for each individual realization, providing a stronger theoretical assurance. Extensive experiments demonstrate that FedAuto consistently outperforms state-of-the-art baselines under diverse connection failure scenarios for both full-parameter and partial-parameter fine-tuning (e.g., LoRA), and even surpasses strategies that rely on complex communication resource optimization.

## I. INTRODUCTION

**F**EDERATED Learning (FL) has emerged as a powerful paradigm for collaboratively training Deep Neural Network (DNN) across distributed edge clients while preserving data privacy. Owing to its privacy-preserving nature, FL has been widely adopted in data-sensitive domains such as healthcare, finance, and edge intelligence [1]–[3]. In conventional FL frameworks, such as FedAvg [4], the server is responsible only for aggregating client updates, while all training is performed at resource-constrained edge devices. This design imposes substantial computational and communication burdens on clients and fails to leverage the abundant computation and storage resources available at the server.

To better exploit the data and computational resources across both server and client tiers, Federated Fine-Tuning (FFT) has recently attracted growing attention [5], [6]. FFT typically follows a two-stage paradigm: a global model is first pre-trained on large-scale public datasets at a resource-rich server, and is then collaboratively fine-tuned across distributed clients using their private data [7]. During the fine-tuning stage, only model updates are exchanged between the server and clients, enabling the incorporation of private knowledge while preserving data privacy [8]. Benefiting from server-side pre-training, FFT significantly reduces both the computational and communication overhead on edge clients compared with conventional FL. Moreover, by integrating domain-specific private data, FFT improves the generalization capability of pre-trained models beyond what can be achieved using public data alone [9].

Despite these advantages, deploying FFT in real-world heterogeneous networks remains challenging. First, FFT inherits the long-standing issue of *data heterogeneity*, which arises not only between public and private datasets but also across private datasets held by different clients. Second, *communication heterogeneity*, a fundamental yet underexplored challenge, further complicates FFT. In practice, as illustrated in Fig. 1, clients may connect to the server via diverse communication infrastructures (e.g., wired, Wi-Fi, 4G, and 5G), resulting in heterogeneous link capacities and reliability. Connection disruptions can occur unpredictably due to device-side factors (e.g., battery depletion or hardware failures) or channel-side conditions (e.g., weak coverage and interference) [10]–[12]. Consequently, clients experience highly heterogeneous disconnection patterns in both frequency and duration. When combined with data heterogeneity, such communication unreliability can severely bias the global optimization process, as clients with more stable connections may disproportionately influence model aggregation. This

Y. Wang, Z. Dai, J. Zhou, and F. Xiao are with the School of Computer Science, Nanjing University of Posts and Telecommunications, Nanjing 210023, China (e-mail: hiwangym@gmail.com, daizhiwen177@foxmail.com, zhoujian@njupt.edu.cn, xiaof@njupt.edu.cn). (Corresponding author: Fu Xiao)

S. Wang are with the National Key Laboratory of Wireless Communications, University of Electronic Science and Technology of China, Chengdu 611731, China (e-mail: shuawaiwang@uestc.edu.cn).

Tony Q. S. Quek is with the Singapore University of Technology and Design, Singapore 487372, and also with the Department of Electronic Engineering, Kyung Hee University, Yongin 17104, South Korea (e-mail: tonyquek@sutd.edu.sg).

T.-H. Chang is with the School of Artificial Intelligence, The Chinese University of Hong Kong, Shenzhen 518172, China (e-mail: tsunghui.chang@ieee.org). (Preprint. Under review.)

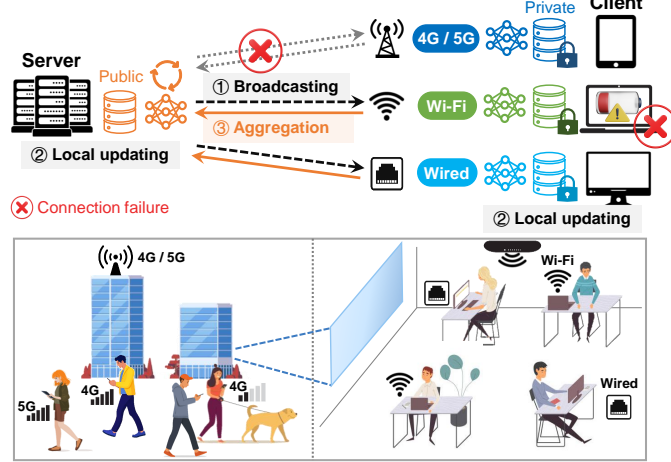


Fig. 1: FFT over heterogeneous and unreliable networks.

bias degrades convergence and generalization performance of FFT, and the empirical evidence supporting this can be found in Section II-C.

Existing approaches for mitigating data heterogeneity primarily focus on conventional FL settings, where all training data reside exclusively on edge clients [13]–[15]. As such methods do not account for the mixed public-private data structure inherent in FFT, directly applying them may underutilize FFT’s unique data-distribution characteristics. Meanwhile, most studies addressing communication unreliability in FL either assume homogeneous network standards or rely on accurate prior knowledge of connection failure probabilities. Physical-layer communication resource optimization approaches, such as transmit power and bandwidth allocation [10], [16]–[18], are often impractical in heterogeneous commercial networks spanning diverse communication standards. In contrast, client selection strategies [19]–[21] heavily depend on accurate estimation of time-varying failure probabilities, which is difficult to achieve in practice. These limitations highlight the need for an FFT framework that is robust to both data heterogeneity and unpredictable communication unreliability, while remaining easy to deploy over existing heterogeneous commercial networks.

#### A. Related work

Since the distributed fine-tuning stage of FFT closely resembles conventional FL, consisting of distributed training and global aggregation, we review related work in both areas.

1) *Data Heterogeneity*: Data heterogeneity is a long-standing challenge in FL and has been extensively studied [2], [13]–[15], [22], [23]. Representative methods include FedProx [22], which introduces a proximal regularization term to stabilize local updates, and SCAFFOLD [23], which mitigates client drift using control variates. However, these methods are designed for conventional FL and assume that all training data reside on edge clients, making them ill-suited for FFT’s mixed public-private data setting. Recent FFT-specific methods, such as FedIT [5], FLORA [24], and FedEx-LoRA [25], consider data heterogeneity during aggregation of fine-tuned parameters. Nevertheless, they still overlook the role of server-side public data in the overall FFT process and assume ideal, lossless communication between the server and clients. These assumptions limit their applicability in practical unreliable network environments.

2) *Connection Unreliability*: To mitigate the effects of communication unreliability in FL, one line of work focuses on optimizing physical-layer resources such as transmit power and bandwidth. For example, [16] optimizes transmit power and bandwidth allocation in Frequency Division Multiple Access (FDMA) systems, which [17], [18], and [26] jointly optimize transmit power and bandwidth together with quantization bit allocation, communication latency, and model adaptation, respectively. Although effective, these approaches require centralized control over communication resources, which is often infeasible in heterogeneous commercial networks with diverse communication standards and device-specific configurations.

Another line of research addresses unreliability through client selection without modifying network infrastructure. F3AST [19] balances long-term client participation by assuming that clients’ successful connection probabilities follow a homogeneous Markov chain, while [20] and FedCote [21] explicitly incorporate connection failure probabilities into the optimization of client selection policies. However, these methods rely on accurate estimation of connection failure probabilities, which is challenging in practice due to time-varying channels and diverse failure modes. More recently, FedAWE [27] removes this requirement but adjusts local step sizes based on connection failure counts, rendering it ineffective under prolonged disconnections.

3) *Personalized FL*: Beyond FFT, personalized FL aims to improve each client’s individual model by adapting to its local data distribution, rather than learning a single global model [28], [29]. Similar to FFT, communication reliability also plays

a critical role in personalized FL, as clients with more stable connections may dominate the aggregation of globally shared parameters. Despite its practical importance, robustness to heterogeneous and unreliable communication remains underexplored in personalized FL.

### B. Contributions

This paper aims to enhance the robustness of FFT in heterogeneous and unreliable network environments that reflect real-world commercial communication systems, characterized by diverse network standards and unpredictable connection failures. To this end, we propose **FedAuto**, a novel FFT framework that mitigates the joint effects of data heterogeneity and connection unreliability through adaptive aggregation alone, without requiring network infrastructure modification or prior knowledge of failure probabilities.

Our main contributions are summarized as follows:

- 1) **FFT under heterogeneous and unreliable networks:** We systematically study FFT under realistic network conditions with heterogeneous communication standards and diverse connection failure patterns. To the best of our knowledge, this is the first work to jointly consider these challenges in FFT.
- 2) **FedAuto:** We propose FedAuto, an adaptive aggregation strategy that alleviates the adverse effects of both data heterogeneity and connection unreliability. FedAuto operates solely at the aggregation level and enables plug-and-play deployment over existing commercial networks.
- 3) **Convergence guarantee:** We theoretically characterize the joint effects of aggregation weights, data heterogeneity, and connection failures on FFT convergence. To the best of our knowledge, this is the first analysis to explicitly reveal the impact of aggregation weights under unreliable networks. Moreover, by adopting a novel per-round aggregation perspective, our analysis eliminates the need for assumptions on connection failures probabilities or client selection strategies that are commonly imposed in conventional analyses. Consequently, it guarantees convergence of the proposed FedAuto for each individual realization, providing a stronger theoretical assurance.
- 4) **Extensive experiments:** We conduct comprehensive experiments on fine-tuning pre-trained models of varying scales (CNNs, ResNets, and ViTs) across multiple datasets and diverse connection failure scenarios. The results demonstrate that FedAuto consistently outperforms existing baselines and even surpasses communication resource allocation-based methods without any network-level intervention.

**Synopsis:** The remainder of this paper is organized as follows. Section II introduces the FFT framework under unreliable network connections. Section III presents the proposed adaptive aggregation strategy, FedAuto. Section IV provides the theoretical convergence analysis. Section V reports the experimental results. Finally, Section VI concludes the paper and discusses future research directions.

## II. FEDERATED FINE-TUNING UNDER UNRELIABLE CONNECTIONS

### A. Learning Objective for FFT

We consider a practical distributed learning setting, illustrated in Fig. 1, in which an edge server maintains a public dataset and each client holds a private dataset. The server's public dataset typically provides broad class coverage but contains only a limited number of samples per class. In contrast, each client's private dataset is domain-specific, with narrower class coverage but substantially higher sample density for the categories it contains. Such a heterogeneous data distribution is common in real-world deployments. Public datasets are often constructed from diverse online sources and thus lack domain specificity. Meanwhile, clients—such as hospitals or banks—possess rich, well-curated data that are restricted to specific domains (e.g., X-ray images for a particular disease or financial documents of a specific type), but these data cannot be shared due to privacy or regulatory constraints.

To leverage both the general knowledge contained in the server-side public dataset and the domain-specific information in the client-side private datasets, the server collaborates with  $N$  clients to solve the following global learning objective:

$$\min_{\mathbf{w}} F_g(\mathbf{w}; \mathcal{D}_g) = p_s F_s(\mathbf{w}; \mathcal{D}_s) + \sum_{i=1}^N p_i F_i(\mathbf{w}; \mathcal{D}_i), \quad (1)$$

where  $\mathcal{D}_s$  is the server's public dataset,  $\mathcal{D}_i$  is the private dataset of client  $i \in [N]$ , and  $\mathcal{D}_g \triangleq \mathcal{D}_s \bigcup (\cup_{i=1}^N \mathcal{D}_i)$  denotes the global dataset combining both public and private data.  $\mathbf{w}$  represents the model parameters to be learned. The weight coefficients  $p_s = |\mathcal{D}_s|/|\mathcal{D}_g|$  and  $p_i = |\mathcal{D}_i|/|\mathcal{D}_g|$  are proportional to dataset sizes and satisfy  $p_s + \sum_{i=1}^N p_i = 1$ .  $F_g$  denotes the global cost function, while  $F_s$  and  $F_i$  represent the local ones for the server and client  $i$ , respectively.

Directly solving (1) through centralized learning would require all clients to upload their private datasets to the server, which is infeasible in privacy-sensitive settings. FFT addresses this limitation by enabling collaborative training that integrates knowledge from both public and private datasets without accessing or transmitting any raw client data. The detailed FFT procedure is described in the subsequent Section II-B.

### B. FFT Procedure

To integrate the general knowledge in server-side public dataset with the domain-specific information in clients' private datasets, while preserving privacy and reducing both computation and communication overhead on resource-limited clients, FFT adopts a two-stage framework: the server first pre-trains the model on the public dataset, followed by distributed fine-tuning on the clients' private datasets.

1) *Server-Side Pre-Training*: The server first pre-trains a global model on its public dataset  $\mathcal{D}_s$  using centralized learning. In practice, the model can be trained from scratch solely on  $\mathcal{D}_s$ , or obtained by further fine-tuning an existing pre-trained model (e.g., adapting a ViT model pre-trained on ImageNet dataset to the CIFAR-100 classification task [30]). The resulting model, denoted  $\bar{\mathbf{w}}_{\text{pre}}$ , provides a strong initialization for subsequent distributed fine-tuning, substantially reducing clients' computational and communication costs by avoiding training from scratch.

2) *Distributed Fine-Tuning*: The distributed fine-tuning stage follows the standard FL paradigm. It further enhances the generalization ability of the pre-trained model  $\bar{\mathbf{w}}_{\text{pre}}$  by integrating knowledge from both public and private datasets. During fine-tuning, the model parameters updated may include the full model (i.e., full-parameter fine-tuning) or only a subset (e.g., LoRA-based fine-tuning [31]). As illustrated in Fig. 1, each communication round  $r$  consists of the following steps:

- (a) **Broadcasting**: The server selects a subset of clients  $\mathcal{K}_r \subseteq [N]$  with  $|\mathcal{K}_r| = K$  and broadcasts the current global model  $\bar{\mathbf{w}}_{r-1}$  to them, where the initial model is set as  $\bar{\mathbf{w}}_0 = \bar{\mathbf{w}}_{\text{pre}}$ .
- (b) **Local updating**: Each selected client  $i \in \mathcal{K}_r$  initializes its local model as  $\mathbf{w}_i^{r,0} = \bar{\mathbf{w}}_{r-1}$  and performs  $E$  steps of gradient descent<sup>1</sup> on its private dataset  $\mathcal{D}_i$ :

$$\mathbf{w}_i^{r,t} = \mathbf{w}_i^{r,t-1} - \gamma \nabla F_i(\mathbf{w}_i^{r,t-1}; \mathcal{D}_i), \quad t \in [E], \quad (2)$$

where  $\gamma > 0$  is the learning rate. In parallel, the server updates its own local model on the public dataset  $\mathcal{D}_s$  to mitigate forgetting of public-domain knowledge:

$$\mathbf{w}_s^{r,t} = \mathbf{w}_s^{r,t-1} - \gamma \nabla F_s(\mathbf{w}_s^{r,t-1}; \mathcal{D}_s), \quad t \in [E], \quad (3)$$

where the server-side local model is likewise initialized from the previous global model, i.e.,  $\mathbf{w}_s^{r,0} = \bar{\mathbf{w}}_{r-1}$ .

- (c) **Global aggregation**: The server updates the global model by aggregating its own local model together with those received from the selected clients:

$$\bar{\mathbf{w}}_r = \beta_s^r \mathbf{w}_s^{r,E} + \sum_{i \in \mathcal{K}_r} \beta_i^r \mathbf{w}_i^{r,E}, \quad (4)$$

where  $\beta_s^r$  and  $\beta_i^r$  are the aggregation weights for the server and each selected client  $i \in \mathcal{K}_r$ . These weights are nonnegative and satisfy the normalization condition  $\beta_s^r + \sum_{i \in \mathcal{K}_r} \beta_i^r = 1$ . In standard FL schemes such as FedAvg, these weights are assigned uniformly or in proportion to the coefficients  $p_s$  and  $p_i$  in (1). Importantly, during aggregation, only model parameters are transmitted from clients to the server, with no raw data exchanged, thereby preserving data privacy.

**Remark 1** Based on existing convergence analyses [32] and [21], it is straightforward to show that under full client participation ( $K = N$ ), the aggregation scheme in (4) achieves optimality when  $\beta_s^r = p_s$  and  $\beta_i^r = p_i \forall i \in [N]$ , consistent with the distributed objective (1). Under partial participation ( $K < N$ ), assigning uniform weights to selected clients, such as  $\beta_s^r = p_s$  and  $\beta_i^r = (1-p_s)/K \forall i \in \mathcal{K}_r$ , yields an unbiased estimate of the full-participation update:  $\mathbb{E}_{\mathcal{K}_r}[\bar{\mathbf{w}}_r] = p_s \mathbf{w}_s^{r,E} + \sum_{i=1}^N p_i \mathbf{w}_i^{r,E}$ . A detailed proof is provided in Appendix I.

### C. Aggregation under Unreliable Connections

Although the FFT framework described above effectively exploits both the server's public data and the clients' private data to improve global model generalization, it implicitly assumes reliable communication. This assumption is often unrealistic, as real-world networks (Fig. 1) frequently experience unstable connections that disrupt server-client communication and prevent timely model exchange. To capture such connection failures, the aggregation scheme in (4) is revised as

$$\bar{\mathbf{w}}_r = \beta_s^r \mathbf{w}_s^{r,E} + \sum_{i \in \mathcal{K}_r} \mathbf{1}_i^r \beta_i^r \mathbf{w}_i^{r,E}, \quad (5a)$$

$$\text{s.t. } \beta_s^r + \sum_{i \in \mathcal{K}_r} \mathbf{1}_i^r \beta_i^r = 1, \quad (5b)$$

where  $\mathbf{1}_i^r = 1$  denotes a successful server-client transmission and  $\mathbf{1}_i^r = 0$  denotes a failure. By incorporating the revised aggregation rule (4), the complete FFT procedure under unreliable connections is summarized in Algorithm 1.

<sup>1</sup>When using mini-batch stochastic gradient descent (SGD), the full gradient  $\nabla F_i(\mathbf{w}; \mathcal{D}_i)$  in (2) is replaced by  $\nabla F_i(\mathbf{w}; \xi_i^r)$ , where  $\xi_i^r$  denotes a mini-batch sample and the corresponding loss is  $F_i(\mathbf{w}; \xi_i^r) = \mathbb{E}_{\xi \in \xi_i^r} [\mathcal{L}(\mathbf{w}; \xi)]$ . For clarity, the theoretical analysis is based on full gradients, whereas the experiments employ mini-batch SGD.

**Algorithm 1** FFT procedure under unreliable connections

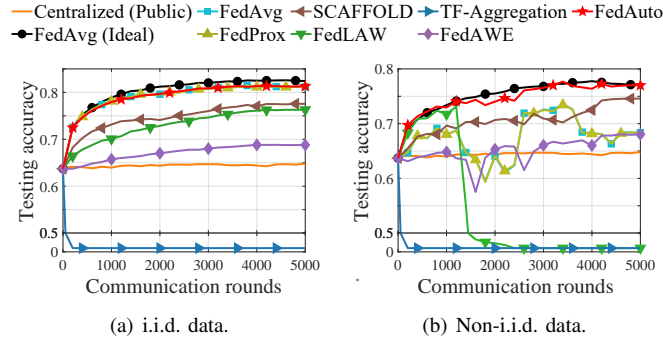
---

```

// Stage 1: Pre-training:
1: Server pre-trains the global model on the public dataset;
// Stage 2: Distributed fine-tuning:
2: for  $r = 1, 2, \dots, R$  do
    // (2-1) Broadcasting:
3:    Server broadcasts global model  $\bar{w}_{r-1}$  to selected clients;
    // (2-2) Local updating:
4:    for each selected client  $i \in \mathcal{K}_r$  and the server do (in parallel)
5:        Update local model via (2) or (3);
6:    end for
    // (2-3) Global Aggregation:
7:    Server aggregates a new global model  $\bar{w}_r$  by (5);
8: end for

```

---

Fig. 2: FFT performance under heterogeneous networks with unreliable connections (CIFAR-10, mixed connection failures,  $K = 20$ ).

#### D. Network Unreliability May Lead to Significant Bias

Similar to Remark 1, the aggregation weights for the global aggregation scheme (5) under unreliable networks can be heuristically assigned either uniformly under partial participation or proportionally to the coefficients  $p_s$  and  $p_i$  in (1) under full participation<sup>2</sup>. However, these heuristic assignments can significantly degrade FFT performance, especially when both connection failures and non-i.i.d. data coexist.

Fig. 2 illustrates this degradation by comparing CIFAR-10 testing accuracy across various FL strategies during distributed fine-tuning under unreliable networks, for both i.i.d. and non-i.i.d. data distributions. The experiment considers a practical heterogeneous network environment, where clients connect to the server via diverse commercial network standards (wired, Wi-Fi, 4G, and 5G), with connection failures including both transient and intermittent disruptions; refer to Section V-A for more detailed experimental settings.

As shown, most FL strategies improve global generalization by utilizing private datasets, outperforming Centralized (Public) (orange curve), which relies solely on the server-side public data. However, both the classical FedAvg and the advanced FedProx [22], which rely on the aforementioned heuristic aggregation weights, degrade significantly under non-i.i.d. data. Similarly, methods for mitigating data heterogeneity (e.g., SCAFFOLD [23]), specialized aggregation schemes such as FedLAW [33], and approaches for handling connection failures (e.g., TF-Aggregation [20] and FedAWE [27]), all exhibit unstable convergence or suboptimal performance, even under i.i.d. data. These results highlight the need to address the combined effects of connection unreliability and data heterogeneity on FFT performance.

To address this issue, Section III introduces FedAuto $\circ$ , a novel FFT framework with adaptive aggregation that mitigates both effects without requiring prior knowledge of connection failures or modifications to existing network infrastructure. Section IV further provides rigorous convergence guarantees, showing that FedAuto $\circ$  achieves robust convergence under heterogeneous and unreliable network conditions. To the best of our knowledge, this is the first work to address unreliable connection issues in FFT within the context of practical heterogeneous networks, involving multiple network standards and diverse connection failure patterns.

### III. ADAPTIVE AGGREGATION STRATEGY

In global aggregation (5), regardless of network standards or connection failure types, the server integrates its own updated local model only with those from successfully connected clients. However, stable FFT convergence requires balanced contribu-

<sup>2</sup> Based on Remark 1 and the normalization condition (5b), the aggregation weights in (5a) can be heuristically set as  $\beta_s^r = \frac{p_s}{p_s + \sum_{j \in [N]} \mathbb{1}_j^r p_j}$  for the server and  $\beta_i^r = \frac{p_i}{p_s + \sum_{j \in [N]} \mathbb{1}_j^r p_j}$  for each successfully connected client (with  $\mathbb{1}_i^r = 1$ ) under full participation, or as  $\beta_s^r = p_s$  and  $\beta_i^r = \frac{1-p_s}{\sum_{j \in \mathcal{K}_r} \mathbb{1}_j^r}$  under partial participation.

tions across data classes [21], [33], which can be disrupted under unreliable connections. In unreliable networks, clients with poor connections may suffer higher transmission failure probabilities, leading to an underrepresentation of their domain-specific knowledge in global aggregation. This becomes particularly problematic when certain classes, primarily owned by clients with unstable connections, are lost, resulting in convergence bias and diminished FFT performance. To address this issue, we propose FedAuto, a novel FFT scheme with adaptive aggregation that mitigates the impact of both connection unreliability and data heterogeneity. The core idea is to use only the server's available resources (i.e., its public dataset and received local models) to balance class contributions and ensure robust convergence, without requiring modifications to existing network infrastructure. This adaptive aggregation strategy consists of two core modules.

### A. Module 1: Server-Side Compensatory Training

In unreliable networks, some class-specific local updates from clients may be missing due to connection failures. Although the server's local model,  $\mathbf{w}_s^{r,E}$ , is trained via (3) on the public dataset  $\mathcal{D}_s$ , which covers a broad range of classes, its uniform contribution across classes is insufficient to specifically compensate for the missing ones in the received clients' updates. Consequently, these classes remain underrepresented during global aggregation in (5). To mitigate this, we propose a compensatory training mechanism that leverages the server's public dataset to enhance the contributions of these missing classes in global aggregation.

Let  $\mathcal{C}_{\text{miss}}^r$  denote the classes missing in received local models from clients in round  $r$ . If  $\mathcal{C}_{\text{miss}}^r \neq \emptyset$ , the server trains a compensatory model  $\mathbf{w}_{\text{miss}}^{r,t}$  using a data subset  $\mathcal{D}_{\text{miss}}^r \subset \mathcal{D}_s$  that contains only samples from the missing classes. Following the update rule in (3), the compensatory model is initialized as  $\mathbf{w}_{\text{miss}}^{r,0} = \bar{\mathbf{w}}_{r-1}$  and updated by  $E$ -step gradient descents:

$$\mathbf{w}_{\text{miss}}^{r,t} = \mathbf{w}_{\text{miss}}^{r,t-1} - \gamma \nabla F_s(\mathbf{w}_{\text{miss}}^{r,t-1}; \mathcal{D}_{\text{miss}}^r), \quad t \in [E]. \quad (6)$$

This procedure is triggered only when missing classes are detected, thus incurring negligible additional cost at the resource-rich server.

With this compensatory mechanism, the global aggregation scheme (5) is refined as

$$\bar{\mathbf{w}}_r = \beta_s^r \mathbf{w}_s^{r,E} + \beta_{\text{miss}}^r \mathbf{w}_{\text{miss}}^{r,t} + \sum_{i \in \mathcal{K}_r} \mathbf{1}_i^r \beta_i^r \mathbf{w}_i^{r,E}, \quad (7)$$

where the aggregation weight of compensatory model,  $\beta_{\text{miss}}^r$ , is set to zero if no classes are missing (i.e.,  $\mathcal{C}_{\text{miss}}^r = \emptyset$ ).

### B. Module 2: Aggregation Weight Optimization

After compensating for missing classes, the next step is to ensure that each class's contribution to global aggregation aligns with its proportion in the global dataset  $\mathcal{D}_g \triangleq \mathcal{D}_s \bigcup (\bigcup_{i=1}^N \mathcal{D}_i)$ , as defined in the learning objective (1). This will be formally justified by the convergence analysis of FFT under unreliable networks (Theorem 1 and Corollary 2) presented in Section IV. Based on the refined aggregation scheme (7), after collecting the updated local models ( $\mathbf{w}_s^{r,E}$  and  $\mathbf{w}_i^{r,E}$ ) and the compensatory model  $\mathbf{w}_{\text{miss}}^{r,t}$  (if present), the server can adjust only the aggregation weights  $\beta_s^r$ ,  $\beta_{\text{miss}}^r$ , and  $\beta_i^r$ . Therefore, to balance each class's contribution to global aggregation, we propose optimizing these weights.

Let  $\alpha_{g,c}$  denote the proportion of class- $c$  samples in the global dataset  $\mathcal{D}_g$ . Similarly, let  $\alpha_{s,c}$ ,  $\alpha_{\text{miss},c}$  and  $\alpha_{i,c}$  represent the class- $c$  proportions in the public dataset  $\mathcal{D}_s$ , the compensatory dataset  $\mathcal{D}_{\text{miss}}^r$ , and the private dataset  $\mathcal{D}_i$ , respectively<sup>3</sup>. We aim to ensure that each class's effective contribution to the global aggregation aligns with its proportion in  $\mathcal{D}_g$ . This leads to the following minimization problem:

$$\min_{\substack{\beta_s^r, \beta_{\text{miss}}^r, \\ \{\beta_i^r\}_{\mathcal{K}_r} = 1}} \sum_{c=1}^C \frac{\left( \alpha_{g,c} - \overbrace{(\beta_s^r \alpha_{s,c} + \beta_{\text{miss}}^r \alpha_{\text{miss},c} + \sum_{i \in \mathcal{K}_r} \mathbf{1}_i^r \beta_i^r \alpha_{i,c})}^{\triangleq \tilde{\alpha}_c^r} \right)^2}{\alpha_{g,c}}, \quad (8a)$$

$$\text{s.t.} \quad \beta_s^r + \beta_{\text{miss}}^r + \sum_{i \in \mathcal{K}_r} \mathbf{1}_i^r \beta_i^r = 1. \quad (8b)$$

Here,  $\tilde{\alpha}_c^r$  represents the effective proportion of class- $c$  samples contributing to the aggregated global model, and  $C$  is the number of classes. The denominator  $\alpha_{g,c}$  prevents minority classes from being neglected. The optimization formulation (8) is a convex weighted least squares problem, which can be easily solved using standard solvers such as CVX [34] or Gurobi [35].

Despite its effectiveness, the optimization formulation (8) has a limitation: when the public dataset  $\mathcal{D}_s$  closely matches the global distribution (i.e.,  $\alpha_{s,c} \approx \alpha_{g,c} \forall c \in [C]$ ), while private datasets remain heterogeneous, the optimization may assign an

<sup>3</sup>From the definition of the global dataset  $\mathcal{D}_g$  in the learning objective (1), its class distribution is the weighted average of the local class distributions, i.e.,  $\alpha_{g,c} = p_s \alpha_{s,c} + \sum_{i=1}^N p_i \alpha_{i,c}$ .

**Algorithm 2** FedAuto: FFT with adaptive aggregation

---

```

// Substitute Step 7 in Algorithm 1:
1: if  $C_{\text{miss}}^r \neq \emptyset$  then
2:   Server performs compensatory training by (6); (Module 1)
3: end if
4: Server optimizes aggregation weights via (8); (Module 2)
5: Server updates the global model  $\bar{\mathbf{w}}_r$  using (7).

```

---

excessively large aggregation weight to the server, thereby underutilizing private updates. To address this, we fix the server's aggregation weight as

$$\beta_s^r = \frac{1}{1 + \sum_{i \in \mathcal{K}_r} \mathbb{1}_i^r}, \quad (9)$$

where  $\sum_{i \in \mathcal{K}_r} \mathbb{1}_i^r$  is the number of clients successfully connected in round  $r$ . This constraint ensures proportional contribution from the server's public dataset while enabling the global model to continuously integrate knowledge from private datasets, thereby enhancing generalization.

The complete procedure of FedAuto is summarized in Algorithm 2. Since the adaptive aggregation strategy is fully executed on the server, FedAuto can be seamlessly integrated into existing systems without requiring modifications to the underlying network infrastructure.

**Remark 2** To solve (8), clients only need to share their local class distributions  $\{\alpha_{i,c}\}$ , which reveal minimal private information. If stronger privacy guarantees are required, techniques such as secure multiparty computation can be applied [36]. As this work focuses on mitigating the effects of connection unreliability on FFT performance, privacy-preserving mechanisms are not further elaborated.

**Remark 3** This work assumes that the server has access to public data covering all client-owned classes, obtained from online resources [37] or generated using GANs [38] or diffusion models [39]. Under this assumption, the server can fully compensate for missing classes during compensatory training (Module 1). Future work may relax this assumption by considering scenarios in which some classes are unavailable at the server. In such cases, class-incremental learning techniques [40], [41], combined with data generation techniques, could be employed to mitigate class unavailability.

#### IV. CONVERGENCE ANALYSIS OF FFT

In this section, we analyze the convergence of the proposed FedAuto. We present a novel per-round aggregation view for FFT analysis, which removes the need for assumptions regarding the types and probabilities of connection failures, as well as the client selection strategies. Unlike existing analyses that establish convergence only in expectation under unreliable networks, our approach ensures that the proposed FedAuto converges for each individual realization, thereby providing a stronger theoretical guarantee. We first introduce two key foundations for deriving FFT convergence: the per-round view of global aggregation and the underlying causes of data heterogeneity. Building on these, we derive the FFT convergence rate under unreliable connections, which establishes the theoretical convergence guarantee of FedAuto.

##### A. Per-Round View of Global Aggregation

In the global aggregation scheme (5) for FFT, both connection reliability (i.e.,  $\mathbb{1}_i^r$ ) and client selection (i.e.,  $\mathcal{K}_r$ ) directly influence the aggregated global model. Existing convergence analyses of FL under unreliable networks typically assume simplified models for connection failures (e.g., packet error rate [16] or transmission outage probability [17], etc) and fixed client selection strategies (e.g., full or partial participation, with or without replacement [20], [21]). These assumptions enable estimation of the expected global model,  $\mathbb{E}_{\mathcal{K}_r, \mathbb{1}_i^r}[\bar{\mathbf{w}}_r]$ , and provide convergence guarantees *in expectation*.

However, such expectation-based approaches often fail to generalize well in real-world heterogeneous networks. On one hand, connection unreliability arises from complex and mixed failure types [33]. On the other hand, client selection strategies vary across network standards and rarely follow uniform rules [42]. Moreover, both connection reliability and client participation probabilities evolve dynamically due to client mobility and fluctuating communication conditions. As a result, accurately modeling these probabilities throughout the training process is highly challenging.

To overcome these limitations, we adopt a *per-round aggregation view* that embeds the combined effects of connection unreliability and client selection into the aggregation weights. This reformulation eliminates the need for explicit modeling of connection failure probabilities or predefined client selection strategies in FFT convergence analysis. The key insight is formalized as follows:

**Proposition 1** In each communication round, regardless of the connection failure type or client selection strategy, the aggregated global model in (5) can be reformulated based on the actual contribution of each client as

$$\bar{\mathbf{w}}_r = \beta_s^r \mathbf{w}_s^{r,E} + \sum_{i=1}^N \beta_i^r \mathbf{w}_i^{r,E}, \quad (10a)$$

$$s.t. \quad \beta_s^r \geq 0, \quad (10b)$$

$$\beta_i^r \geq 0 \text{ if } i \in \mathcal{K}_r \text{ and } \mathbf{1}_i^r = 1; \quad \beta_i^r = 0 \text{ otherwise,} \quad (10c)$$

$$\beta_s^r + \sum_{i=1}^N \beta_i^r = 1. \quad (10d)$$

Here, the constraint (10c) incorporates the effects of both network unreliability and client selection into the aggregation weight  $\beta_i^r$ , which reflects each client's actual contribution to the global model in round  $r$ . Only the clients with successful connections contribute to the global model, while those unselected or disconnected have  $\beta_i^r = 0$ .

### B. Causes of Data Heterogeneity

As indicated by (10a), the convergence direction of the aggregated global model depends not only on the aggregation weights  $\beta_s^r$  and  $\beta_i^r$ , but also on the local models  $\mathbf{w}_s^{r,E}$  and  $\mathbf{w}_i^{r,E}$ . From the update rules in (2) and (3), each local model is updated along its corresponding gradient, i.e.,  $\nabla F_s(\mathbf{w}; \mathcal{D}_s)$  for the server and  $\nabla F_i(\mathbf{w}; \mathcal{D}_i)$  for each client  $i \in [N]$ . These gradients are determined by the data distributions of public dataset  $\mathcal{D}_s$  and private datasets  $\mathcal{D}_i$ , all of which serve as local datasets in FFT under the learning objective defined in (1).

In contrast, the global gradient  $\nabla F_g(\mathbf{w}; \mathcal{D}_g)$ , derived from the global objective (1), characterizes the ideal convergence direction of the fine-tuned global model. It is determined by the data distribution of the global dataset  $\mathcal{D}_g$ , which integrates all local datasets. Consequently, discrepancies between local and global data distributions inherently induce deviations between their gradients. For this reason, the gradient gaps  $\|\nabla F_s(\mathbf{w}) - \nabla F(\mathbf{w})\|^2$  and  $\|\nabla F_i(\mathbf{w}) - \nabla F(\mathbf{w})\|^2$  are widely used to quantify data heterogeneity in FL convergence analyses, especially in non-convex settings [1], [17], [23]. Prior studies consistently indicate that greater data heterogeneity significantly degrades convergence speed.

To more precisely characterize the impact of data heterogeneity on FFT performance, we adopt the decomposition framework from our prior work [21], which separates data heterogeneity into feature-related and label-related components. Specifically, the global and local gradients can be reformulated as class-wise weighted averages:

$$\nabla F_g(\mathbf{w}) = \sum_{c=1}^C \alpha_{g,c} \nabla F_{g,c}(\mathbf{w}), \quad (11a)$$

$$\nabla F_j(\mathbf{w}) = \sum_{c=1}^C \alpha_{j,c} \nabla F_{j,c}(\mathbf{w}), \quad j \in \{s, [N]\}, \quad (11b)$$

with  $j = s$  denoting the server and  $j \in [N]$  each client. Here,  $\nabla F_{g,c}$  and  $\nabla F_{j,c}$  are the class- $c$  gradients computed on the global and local datasets, respectively;  $\alpha_{g,c}$  and  $\alpha_{j,c}$  are the corresponding class proportions; and  $C$  is the total number of classes. This reformulation yields the following upper bound on the discrepancy between local and global gradients.

**Proposition 2** [21, Proposition 1] The difference between a local gradient and the global gradient satisfies

$$\|\nabla F_j(\mathbf{w}) - \nabla F_g(\mathbf{w})\|^2 \leq 2 \left( \underbrace{\sum_{c=1}^C \alpha_{j,c} \|\nabla F_{j,c}(\mathbf{w}) - \nabla F_{g,c}(\mathbf{w})\|^2}_{(12a) \text{ related to data feature}} + \underbrace{\chi_{\alpha_j \parallel \alpha_g}^2 \sum_{c=1}^C \alpha_{g,c} \|\nabla F_{g,c}(\mathbf{w})\|^2}_{(12b) \text{ related to sample label}} \right) \quad (12)$$

for  $j = s$  (server) and  $j \in [N]$  (clients). Term (12a) characterizes **feature-related heterogeneity**, where the within-class gradient deviation  $\|\nabla F_{j,c}(\mathbf{w}) - \nabla F_{g,c}(\mathbf{w})\|^2$  arises from factors such as limited local samples and cross-source feature shift [43], [44]. Term (12b) represents **label-related heterogeneity**, where the chi-square divergence  $\chi_{\alpha_j \parallel \alpha_g}^2 \triangleq \sum_{c=1}^C \frac{(\alpha_{j,c} - \alpha_{g,c})^2}{\alpha_{g,c}}$  quantifies the mismatch between local and global class distributions.

*Proof:* See [21, Appendix A]. ■

### C. Convergence Rate of FFT under Unreliable Connections

1) **Assumptions:** Based on Proposition 2, to separately analyze the effects of feature-related heterogeneity and label-related heterogeneity on FFT convergence under unreliable connections, we introduce the following assumptions:

**Assumption 1 (Bounded gradient deviation within a class)** For each class  $c$ , the deviation between a local gradient and the corresponding global gradient is bounded as  $\|\nabla F_{j,c}(\mathbf{w}) - \nabla F_{g,c}(\mathbf{w})\|^2 \leq V_{j,c}^2$ ,  $\forall j \in \{s, [N]\}$ , with  $j = s$  denotes the server and  $j \in [N]$  denotes each client.

**Assumption 2 (Bounded gradient norm)** The global gradient norm is bounded as  $\|\nabla F_g(\mathbf{w})\|^2 \leq G^2$ .

Combining Proposition 2 with Assumptions 1 and 2 yields Corollary 1, which quantifies the degree of data heterogeneity.

**Corollary 1** Under Assumptions 1 and 2, the difference between the local and global gradients is bounded by

$$\|\nabla F_i(\mathbf{w}) - \nabla F(\mathbf{w})\|^2 \leq 2 \sum_{c=1}^C \alpha_{i,c} V_{i,c}^2 + 2\chi_{\alpha_i \parallel \alpha_g}^2 G^2, \quad (13)$$

where the first term on the right-hand side (RHS) of (13) captures the impact of feature-related heterogeneity, and the second term reflects the effect of label-related heterogeneity.

In addition to Assumptions 1 and 2, we adopt the following standard smoothness assumption on local cost functions:

**Assumption 3 (L-smoothness)** Each local cost function is differentiable with Lipschitz-continuous gradients, i.e., there exists a constant  $L > 0$  such that  $\forall \mathbf{w}$  and  $\mathbf{w}'$ ,  $\|\nabla F_j(\mathbf{w}) - \nabla F_j(\mathbf{w}')\|_2 \leq L\|\mathbf{w} - \mathbf{w}'\|_2$ ,  $\forall j \in \{s, [N]\}$ .

2) **Theoretical Results:** The main convergence result for the FFT procedure under unreliable connections, as described in Algorithm 1, is presented below.

**Theorem 1** Suppose Assumptions 1 to 3 hold, and incorporate Propositions 1 and 2. Assume the total number of gradient descent updates  $T = RE$  is sufficiently large with  $T \geq N^3$ , while the number of local update steps  $E$  remains relatively small with  $E \leq T^{\frac{1}{4}}/N^{\frac{3}{4}}$ , where  $R$  is the number of iterations in Algorithm 1. If the learning rate is chosen as  $\gamma = N^{\frac{1}{2}}/(2LT^{\frac{1}{2}})$ , then the convergence of FFT under unreliable connections in Algorithm 1 is upper bounded by

$$\begin{aligned} \frac{1}{R} \sum_{r=1}^R \|\nabla F_g(\bar{\mathbf{w}}_{r-1})\|^2 &\leq \frac{20L}{\sqrt{TN}} (F(\bar{\mathbf{w}}_{\text{pre}}) - F(\bar{\mathbf{w}}_R)) + \underbrace{\frac{8}{\sqrt{TN}R} \sum_{r=1}^R \sum_{j \in \{s, [N]\}} \beta_j^r \sum_{c=1}^C (\alpha_{j,c} V_{j,c}^2 + \chi_{\alpha_g \parallel \alpha_j}^2 G^2)}_{(14a) \text{ caused by non-i.i.d. data}} \\ &\quad + \underbrace{20 \left( \chi_{\mathbf{p} \parallel \beta}^2 \sum_{c=1}^C \sum_{j \in \{s, [N]\}} p_i \alpha_{j,c} V_{j,c}^2 + \frac{1}{R} \sum_{r=1}^R \chi_{\alpha_g \parallel \tilde{\alpha}^r}^2 G^2 \right)}_{(14b) \text{ caused by connection unreliability and non-i.i.d. data}}. \end{aligned} \quad (14)$$

Here, the chi-square divergence  $\chi_{\mathbf{p} \parallel \beta}^2 \triangleq \sum_{j \in \{s, [N]\}} \frac{(\beta_j^r - p_j)^2}{p_j}$  measures the deviation between the aggregation weights  $\{\beta_j^r\}$  and the weight coefficients  $\{p_j\}$  defined in (1). Similarly,  $\chi_{\alpha_g \parallel \tilde{\alpha}^r}^2 \triangleq \sum_{c=1}^C \frac{(\alpha_{g,c} - \sum_{j \in \{s, [N]\}} \beta_j^r \alpha_{j,c})^2}{\alpha_{g,c}}$  quantifies the divergence between the global class distribution  $\{\alpha_{g,c}\}$  and the effective class distribution  $\{\tilde{\alpha}_c^r (\triangleq \sum_{j \in \{s, [N]\}} \beta_j^r \alpha_{j,c})\}$ . The aggregation weights  $\{\beta_j^r\}$  satisfy the constraints (10b)–(10d).

*Proof:* Unlike prior analyses of FL convergence under unreliable networks [16], [19]–[21], we analyze FFT from a per-round aggregation perspective (Proposition 1). This perspective offers two key advantages. First, it eliminates the need to assume specific connection failure models or probabilities, thereby enhancing applicability to practical heterogeneous network environments. Second, while previous works establish convergence only in expectation, we analyze convergence for each individual realization, providing a strictly stronger theoretical result and facilitating the design of more robust FFT strategies under unreliable connections. The full proof is presented in Appendix II. ■

From the RHS of (14), the convergence rate of Algorithm 1 is governed by several key factors, including: (i) aggregation weights of the server and clients ( $\beta_s^r$  and  $\beta_i^r$ ); (ii) data heterogeneity terms ( $V_{i,c}^2$  and  $\chi_{\alpha_i \parallel \alpha_g}^2$ ); and (iii) divergence terms induced by connection unreliability ( $\chi_{\mathbf{p} \parallel \beta}^2$  and  $\chi_{\alpha_g \parallel \tilde{\alpha}^r}^2$ ). Analyzing these terms leads to several important observations:

(a) **Fully reliable connections:** When all connections are reliable and full client participation holds (i.e.,  $\mathbb{1}_i^r = 1 \forall i, r$  and  $\mathcal{K}_r = [N]$ ), choosing aggregation weights consistent with the distributed objective in (1), namely  $\beta_j^r = p_j \forall j \in \{s, [N]\}$ ,

eliminates both divergence terms  $\chi_{\mathbf{p} \parallel \beta}^2$  and  $\chi_{\alpha_g \parallel \tilde{\alpha}^r}^2$ . As a result, term (14b) vanishes, and convergence is still affected by data heterogeneity through term (14a).

- (b) **i.i.d. datasets:** If all local datasets (including both public and private) are i.i.d., their class distributions match the global distribution (i.e.,  $\alpha_{j,c} = \alpha_{g,c}$ ), and the within-class gradient deviations  $\{V_{j,c}^2\}$  become negligible. In this case, both terms (14a) and (14b) disappear, showing that i.i.d. data mitigates the negative effects of connection unreliability and ensures stable convergence.
- (c) **Joint effect of unreliability and heterogeneity:** Term (14b), which captures the joint impacts of connection unreliability and data heterogeneity, does not decay as  $T$  increases. This implies that network unreliability amplifies the adverse effects of data heterogeneity through the divergence factors  $\chi_{\mathbf{p} \parallel \beta}^2$  and  $\chi_{\alpha_g \parallel \tilde{\alpha}^r}^2$ , resulting in biased FFT convergence.
- (d) **Dominance of label-related heterogeneity:** Empirical evidence in [21, Observation 1] shows that under non-i.i.d. data with heterogeneous class distributions, the global gradient norm  $G^2$  is typically several orders of magnitude larger than the average within-class gradient deviation,  $\sum_{j \in \{s, [N]\}} p_i \alpha_{j,c} V_{j,c}^2$ . Consequently, the label-related component  $\frac{1}{R} \sum_{r=1}^R \chi_{\alpha_g \parallel \tilde{\alpha}^r}^2 G^2$  in (14b) dominates the convergence bias. Therefore, enforcing  $\chi_{\alpha_g \parallel \tilde{\alpha}^r}^2 = 0$  in every communication round can eliminate this bias, rendering term (14b) negligible and enabling FFT to converge properly even under unreliable connections.

**Remark 4** To the best of our knowledge, Theorem 1 provides the first theoretical characterization of how aggregation weights influence FFT convergence under unreliable connections. Moreover, it is the first to establish convergence in such settings without requiring prior knowledge of connection failure types or probabilities, making it well suited for real-world FFT deployments in heterogeneous networks.

**Remark 5** If the connection failure probabilities and client selection are explicitly specified, Theorem 1 reduces to expectation-based convergence analyses such as [20], [21]. In this case, left-hand side (LHS) of (14) becomes  $\frac{1}{R} \sum_{r=1}^R \mathbb{E}_{\mathcal{K}_r, \mathbf{1}_i^r} [\|\nabla F_g(\bar{\mathbf{w}}_{r-1})\|^2]$ , indicating that the proposed analytical framework is more general and subsumes prior convergence results as special cases.

#### D. Convergence Guarantee of FedAuto

From the observation (d) of Theorem 1, proper FFT convergence critically depends on minimizing the divergence between the global and effective class distributions,  $\chi_{\alpha_g \parallel \tilde{\alpha}^r}^2$ , in each round. The proposed FedAuto in Algorithm 2 achieves this through server-side compensatory training for underrepresented classes and adaptive optimization of aggregation weights to balance class contributions in the aggregated global model. As a result, the effective class proportion  $\tilde{\alpha}_c^r$  closely matches the global proportion  $\alpha_{g,c}$  for each class  $c$ , driving  $\chi_{\alpha_g \parallel \tilde{\alpha}^r}^2$  towards zero. This leads to the following result:

**Corollary 2** *Under the conditions of Theorem 1 and incorporating [21, Observation 1], if the adaptive aggregation strategy in Algorithm 2 is employed such that the effective class distribution  $\{\tilde{\alpha}_c^r\}$  closely approximates the global class distribution  $\{\alpha_{g,c}\}$ , i.e.,  $\chi_{\alpha_g \parallel \tilde{\alpha}^r}^2 \approx 0$ , then the convergence rate in (14) approximately reduces to*

$$\frac{1}{R} \sum_{r=1}^R \|\nabla F_g(\bar{\mathbf{w}}_{r-1})\|^2 \lesssim \frac{20L}{\sqrt{TN}} (F(\bar{\mathbf{w}}_{\text{pre}}) - F(\bar{\mathbf{w}}_R)) + \frac{8}{\sqrt{TN}R} \sum_{r=1}^R \sum_{j \in \{s, [N]\}} \beta_j^r \sum_{c=1}^C (\alpha_{j,c} V_{j,c}^2 + \chi_{\alpha_g \parallel \alpha_j}^2 G^2). \quad (15)$$

From the RHS of (15), the global gradient satisfies  $\nabla F_g(\bar{\mathbf{w}}_{r-1}) \rightarrow 0$  as  $T \rightarrow \infty$ , indicating that FFT converges to a proper solution even in the presence of both unreliable connections and data heterogeneity. This establishes a rigorous theoretical convergence guarantee for FedAuto. Moreover, since convergence is ensured for each individual realization rather than only in expectation, FedAuto exhibits strong robustness in unreliable network environments.

**Remark 6** An alternative to adjusting aggregation weights to minimize  $\chi_{\tilde{\alpha} \parallel \alpha_g}^2$  is to modify the local label distributions  $\{\alpha_{i,c}\}$ , for example, through augmenting local datasets with server-side public or synthetic data [45], [46]. Such approaches implicitly render all datasets approximately i.i.d., thereby mitigating the impact of connection unreliability and enabling stable convergence, as noted in the observation b of Theorem (1). However, they incur additional computational and storage overhead on clients, making them less suitable for resource-constrained edge devices. Regardless of the strategy, the core objective remains to balance the effective class distribution  $\{\tilde{\alpha}_c^r\}$  during global aggregation, preventing dominance by overrepresented classes while preserving the contributions of underrepresented ones.

## V. EXPERIMENTAL RESULTS

### A. Parameter Settings

1) *Heterogeneous Network Environment:* We simulate a practical heterogeneous network scenario in which clients connect to the server via diverse communication standards, including wired Ethernet and wireless links over 4G, 5G, and Wi-Fi (2.4 GHz and 5 GHz). As illustrated in Fig. 1, the 4G and 5G base stations are deployed outdoors at the center of a 200 m-radius cell

with an antenna height of 20 m, while the Wi-Fi Access Point (AP) is installed indoors at the center of a  $20 \times 20$  m area with a height of 3 m. The central server coordinates  $N = 20$  clients for FFT of DNNs. Among them, 8 clients are uniformly distributed indoors, and the remaining 12 clients are uniformly distributed in the outdoor region. Detailed network standards and communication resource allocations for each client are provided in Appendix III-A.

2) *Modes of Connection Failures*: We consider three patterns of connection failures:

- **Transient**: Short, random disruptions modeled as instantaneous events with stochastic occurrence. In our experiments, each client's transient failure is induced by transmission outages and its probability is determined by a classical path-loss model with shadowing effects [47].
- **Intermittent**: Longer disruptions (e.g., power depletion) that occur randomly and persist for a duration. Intermittent failure occurrences follow an exponential distribution, while the disconnection durations follow a uniform distribution once triggered [48].
- **Mixed**: A composite mode in which clients experience both transient and intermittent failures.

The full mathematical formulations of these failure models are provided in Appendix III-B.

3) *Datasets, Data Distributions, and Models*: We evaluate FedAuto on three widely used image-classification benchmarks under both i.i.d. and non-i.i.d. data settings. For each dataset, we consider two representative DNNs, one small-scale and one large-scale.

- **MNIST** [49]: 60,000 training and 10,000 test images from ten classes. The i.i.d. setting shuffles and uniformly partitions samples across clients. For the non-i.i.d. setting, each client receives data from two designated classes (e.g., clients 1–4: {1,2}; clients 5–8: {3,4}, etc). For classification, we adopt a small-scale CNN architecture with two convolutional layers followed by fully connected layers (0.22 M parameters), and a large-scale ViT model (86 M parameters).
- **CIFAR-10** [50]: 50,000 training and 10,000 test images from ten classes. Both i.i.d. and non-i.i.d. partitioning follow the MNIST setup. ResNet with Group Normalization (GN) [51] (0.27 M parameters) is used as the small-scale model, and ViT (86 M parameters) as the large one.
- **CIFAR-100** [50]: 50,000 training and 10,000 test images from 100 classes. The i.i.d. partitioning mirrors MNIST, whereas in the non-i.i.d. setting, each client receives data from 20 classes. We use the ResNet-18 model with GN from [51] (11 M parameters) as the small model and again adopt ViT (86 M parameters) as the large one.

The architectures of all employed DNNs are detailed in Appendix III-C. In all experiments, the global model produced by FFT is evaluated on the full test dataset to assess convergence and generalization performance.

4) *Fine-Tuning Strategies*: We compare two strategies:

- **Full-parameter fine-tuning**: All model parameters are updated during training and used for small-scale models.
- **Partial-parameter fine-tuning**: Only a subset of parameters is updated using LoRA [31]. This strategy is employed to fine-tune large-scale ViT models initialized from an ImageNet-1k-pretrained ViT model [52].

The training hyperparameters for both strategies are summarized in Appendix III-D.

5) *Baselines*: To comprehensively assess the effectiveness of FedAuto, we compare it against a broad set of baselines spanning centralized learning, classical FL algorithms, aggregation-enhanced methods, and communication resource-aware schemes. We begin with the centralized learning setting:

- **Central (Public)**: A centralized training scheme in which the server learns the model solely from the public dataset, without leveraging any distributed private data.

We next include classical and the advanced FL algorithms designed to address data heterogeneity:

- **FedAvg (Ideal)** [4]: The classical FedAvg executed without connection failures. It follows Algorithm 1, adopts the aggregation rule in (4), and uses aggregation weights specified in Remark 1. This configuration serves as the performance upper bound in our experiments.
- **FedAvg**: The practical FedAvg deployed under realistic connection failures, implemented via Algorithm 1 using the heuristic aggregation weights defined in footnote 2.
- **FedProx** [22]: An extension of FedAvg that introduces a proximal term into each client's local objective to alleviate the effects of data heterogeneity.
- **SCAFFOLD** [23]: A variance-reduction method that employs control variates on both the server and client sides to correct the client drift induced by non-i.i.d. data.

We further consider aggregation-enhanced methods:

- **FedLAW** [33]: A refinement of FedAvg that leverages a server-side proxy dataset to jointly optimize a global shrinking factor and client-specific aggregation weights, thus enhancing robustness under data heterogeneity.
- **TF-Aggregation** [20]: A method designed to mitigate transient connection failures via incorporating clients' estimated failure probabilities into the global aggregation.
- **FedAWE** [27]: An adaptive weighting scheme that adjusts each client's local stepsize based on its number of failed rounds, thereby balancing global aggregation.
- **FedEx-LoRA** [25]: An enhancement of FedAvg that incorporates the error residual induced by global aggregation of LoRA modules into local model updates.

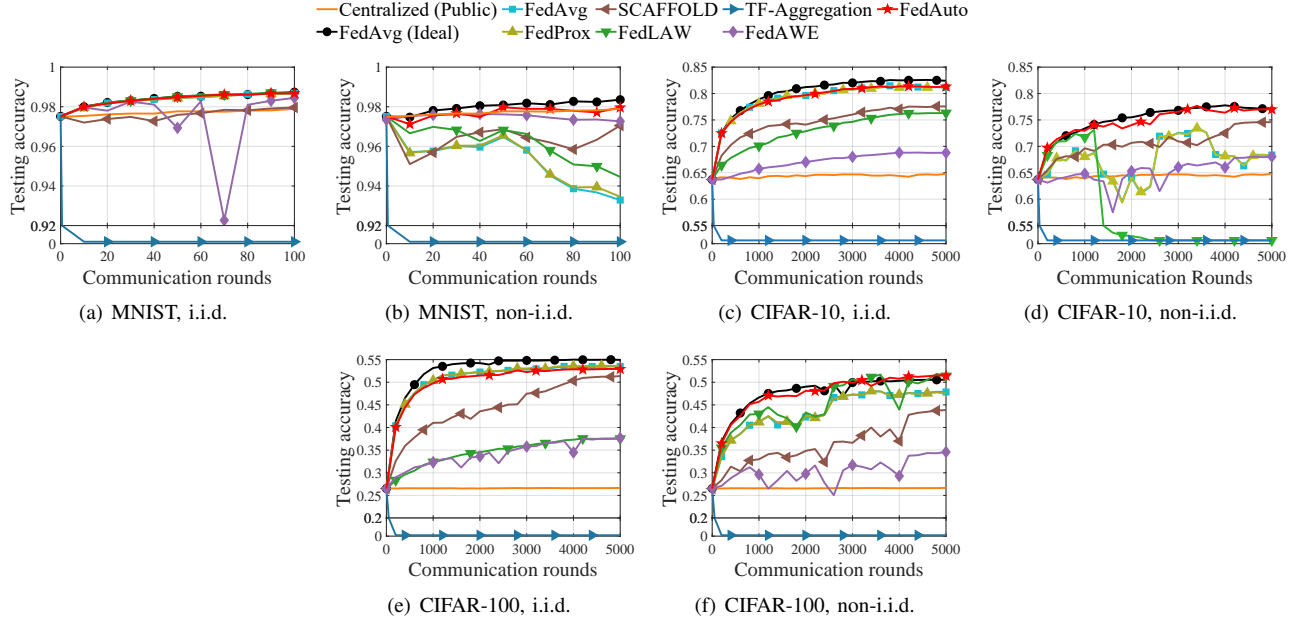


Fig. 3: Convergence of different FFT strategies under full-parameter fine-tuning with full participation ( $K = 20$ , mixed failures).

Table 1: Testing accuracy(%) of different FFT strategies under full-parameter fine-tuning with full participation ( $K = 20$ , i.i.d. data).

FFT Strategy	Transient			Intermittent			Mixed		
	MNIST	CIFAR-10	CIFAR-100	MNIST	CIFAR-10	CIFAR-100	MNIST	CIFAR-10	CIFAR-100
Centralized (Public)	97.89 $\pm$ 0.1337	64.92 $\pm$ 0.9380	26.68 $\pm$ 0.8543	97.89 $\pm$ 0.1337	64.92 $\pm$ 0.9380	26.68 $\pm$ 0.8543	97.89 $\pm$ 0.1337	64.92 $\pm$ 0.9380	26.68 $\pm$ 0.8543
FedAvg [4]	98.70 $\pm$ 0.1330	81.13 $\pm$ 0.3437	51.86 $\pm$ 1.9350	98.65 $\pm$ 0.1236	81.39 $\pm$ 0.4807	53.36 $\pm$ 1.5590	98.68 $\pm$ 0.1251	81.18 $\pm$ 0.4720	53.49 $\pm$ 1.9090
FedProx [22]	98.70 $\pm$ 0.1330	81.01 $\pm$ 0.3503	52.29 $\pm$ 1.7081	98.65 $\pm$ 0.1210	81.35 $\pm$ 0.5428	53.53 $\pm$ 1.7631	98.67 $\pm$ 0.1221	81.12 $\pm$ 0.5482	53.62 $\pm$ 1.7831
SCAFFOLD [23]	97.83 $\pm$ 0.2483	75.49 $\pm$ 0.6683	46.37 $\pm$ 2.2444	98.01 $\pm$ 0.2716	77.09 $\pm$ 0.6215	50.46 $\pm$ 1.3387	97.96 $\pm$ 0.2022	77.55 $\pm$ 0.5254	51.37 $\pm$ 1.5439
FedLAW [33]	98.74 $\pm$ 0.0936	76.66 $\pm$ 1.2494	37.70 $\pm$ 2.8919	98.70 $\pm$ 0.0850	76.65 $\pm$ 1.4020	37.93 $\pm$ 2.4467	98.71 $\pm$ 0.1041	76.32 $\pm$ 1.5242	37.54 $\pm$ 2.7535
TF-Aggregation [20]	9.80 $\pm$ 0.0000	10.00 $\pm$ 0.0000	1.00 $\pm$ 0.0000	9.80 $\pm$ 0.0000	10.00 $\pm$ 0.0000	1.00 $\pm$ 0.0000	9.80 $\pm$ 0.0000	10.00 $\pm$ 0.0000	1.00 $\pm$ 0.0000
FedAWE [27]	91.17 $\pm$ 16.2217	68.84 $\pm$ 0.8884	34.29 $\pm$ 4.1678	98.07 $\pm$ 0.7321	68.84 $\pm$ 0.9319	37.98 $\pm$ 1.3004	98.45 $\pm$ 0.0885	68.78 $\pm$ 1.0224	37.69 $\pm$ 1.2323
<b>FedAuto (Ours)</b>	98.69 $\pm$ 0.0940	81.08 $\pm$ 0.4163	51.48 $\pm$ 1.8997	98.67 $\pm$ 0.1244	81.28 $\pm$ 0.3567	52.67 $\pm$ 1.6424	98.67 $\pm$ 0.1282	81.31 $\pm$ 0.5199	52.90 $\pm$ 1.8059
FedAvg (Ideal)	98.74 $\pm$ 0.1182	82.42 $\pm$ 0.2982	54.95 $\pm$ 1.7194	98.74 $\pm$ 0.1182	82.42 $\pm$ 0.2982	54.95 $\pm$ 1.7194	98.74 $\pm$ 0.1182	82.42 $\pm$ 0.2982	54.95 $\pm$ 1.7194

Finally, we consider FFT-based baselines that explicitly optimize communication resources:

- **ResourceOpt-1:** Motivated by [17, Corollary 1], which indicates that equalizing clients' failure probabilities can reduce convergence bias, this baseline jointly optimizes transmit power and bandwidth to balance transient connection failure probabilities across clients.
- **ResourceOpt-2:** Recognizing that joint optimization of communication resources across multiple standards is often infeasible in heterogeneous commercial networks, this baseline provides a practical variant of ResourceOpt-1 by independently optimizing transmit power and bandwidth allocation within each standard.

Detailed mathematical formulations for the above baselines are provided in Appendix III-E. All reported results are averaged over five independent runs to ensure statistical reliability.

### B. Performance under Full-Parameter Fine-Tuning

In this part, we evaluate the robustness of FedAuto under full-parameter fine-tuning across various combinations of data distributions and connection failure modes.

1) *Full Client Participation:* We first examine various FFT strategies under full client participation with  $K = N = 20$ . The convergence behaviors on multiple datasets are shown in Fig. 3, and the corresponding testing accuracies are summarized in Tables 1 and 2. Since the convergence trends under transient and intermittent failures closely resemble those under the mixed failure mode in Fig. 3, we present them in Appendix IV-A.

**The i.i.d. data case.** From Fig. 3(a), 3(c) and 3(e), together with Table 1, we observe that across all scenarios, FedAuto consistently achieves performance close to the idealized FedAvg (Ideal), which assumes a failure-free network. Most FFT strategies outperform Centralized (Public) (orange curve), which relies exclusively on server-side public data, and this advantage becomes more pronounced on more complex datasets such as CIFAR-10 and CIFAR-100. Moreover, classical FedAvg and advanced FedProx, both adopting aggregation weights aligned with the distributed objective function (1), converge steadily to the optimal solution, in agreement with the observation (b) of Theorem 1.

In contrast, several advanced FFT strategies exhibit unstable convergence or suboptimal performance. SCAFFOLD suffers from performance degradation due to its reliance on dual transmissions of model parameters and control variables, both

Table 2: Testing accuracy(%) of different FFT strategies under full-parameter fine-tuning with full participation ( $K = 20$ , non-i.i.d. data).

FFT Strategy	Transient			Intermittent			Mixed		
	MNIST	CIFAR-10	CIFAR-100	MNIST	CIFAR-10	CIFAR-100	MNIST	CIFAR-10	CIFAR-100
Centralized(Public)	97.89 $\pm$ 0.1337	64.92 $\pm$ 0.9380	26.68 $\pm$ 0.8543	<b>97.89</b> $\pm$ 0.1337	64.92 $\pm$ 0.9380	26.68 $\pm$ 0.8543	97.89 $\pm$ 0.1337	64.92 $\pm$ 0.9380	26.68 $\pm$ 0.8543
FedAvg [4]	96.56 $\pm$ 0.8938	72.82 $\pm$ 1.1859	47.30 $\pm$ 1.3502	94.98 $\pm$ 1.7455	70.33 $\pm$ 1.3170	47.77 $\pm$ 0.9096	93.28 $\pm$ 1.1806	68.35 $\pm$ 0.3418	47.85 $\pm$ 1.0632
FedProx [22]	96.60 $\pm$ 0.8895	72.73 $\pm$ 1.1765	47.36 $\pm$ 1.5320	95.00 $\pm$ 1.7403	70.05 $\pm$ 1.4086	47.76 $\pm$ 0.9871	93.45 $\pm$ 1.3919	68.27 $\pm$ 0.3757	47.54 $\pm$ 1.0059
SCAFFOLD [23]	97.04 $\pm$ 0.9013	72.26 $\pm$ 0.7260	39.80 $\pm$ 1.1494	96.96 $\pm$ 0.5209	<b>74.50</b> $\pm$ 0.5466	42.96 $\pm$ 1.5065	97.05 $\pm$ 0.4798	74.58 $\pm$ 0.4641	43.87 $\pm$ 0.8793
FedLAW [33]	97.24 $\pm$ 0.7967	76.92 $\pm$ 0.9772	32.70 $\pm$ 29.0020	95.80 $\pm$ 1.6932	36.80 $\pm$ 36.7075	<b>54.74</b> $\pm$ 1.0620	94.46 $\pm$ 1.4583	10.00 $\pm$ 0.0000	51.40 $\pm$ 1.4886
TF-Aggregation [20]	9.80 $\pm$ 0.0000	10.00 $\pm$ 0.0000	1.00 $\pm$ 0.0000	9.80 $\pm$ 0.0000	10.00 $\pm$ 0.0000	1.00 $\pm$ 0.0000	9.80 $\pm$ 0.0000	10.00 $\pm$ 0.0000	1.00 $\pm$ 0.0000
FedAWE [27]	73.30 $\pm$ 34.0446	67.16 $\pm$ 1.4748	35.08 $\pm$ 0.8634	73.06 $\pm$ 7.1127	68.34 $\pm$ 0.8812	36.44 $\pm$ 1.0254	67.97 $\pm$ 8.9996	68.05 $\pm$ 1.5370	34.60 $\pm$ 0.5924
<b>FedAuto (Ours)</b>	<b>98.22</b> $\pm$ 0.2499	<b>77.37</b> $\pm$ 0.4824	<b>50.76</b> $\pm$ 1.5694	97.77 $\pm$ 0.2156	<b>76.91</b> $\pm$ 0.6739	51.38 $\pm$ 1.6592	<b>97.96</b> $\pm$ 0.2489	<b>77.00</b> $\pm$ 0.5494	<b>51.43</b> $\pm$ 1.4919
FedAvg (Ideal)	98.35 $\pm$ 0.1599	77.19 $\pm$ 0.7742	50.57 $\pm$ 1.3264	98.35 $\pm$ 0.1599	77.19 $\pm$ 0.7742	50.57 $\pm$ 1.3264	98.35 $\pm$ 0.1599	77.19 $\pm$ 0.7742	50.57 $\pm$ 1.3264

Table 3: Testing accuracy(%) of different FFT strategies under full-parameter fine-tuning with partial participation ( $K = 10$ , mixed failures, non-i.i.d. data).

FFT Strategy	Dataset		
	MNIST	CIFAR-10	CIFAR-100
Centralized(Public)	97.89 $\pm$ 0.1337	64.92 $\pm$ 0.9380	26.68 $\pm$ 0.8543
FedAvg [4]	93.15 $\pm$ 2.5508	67.90 $\pm$ 2.5059	49.28 $\pm$ 1.6928
FedProx [22]	93.10 $\pm$ 2.5112	67.53 $\pm$ 2.5610	48.99 $\pm$ 1.7383
SCAFFOLD [23]	14.64 $\pm$ 8.6962	10.00 $\pm$ 0.0000	1.00 $\pm$ 0.0000
FedLAW [33]	92.39 $\pm$ 3.4460	10.00 $\pm$ 0.0000	1.00 $\pm$ 0.0000
TF-Aggregation [20]	9.80 $\pm$ 0.0000	10.00 $\pm$ 0.0000	1.00 $\pm$ 0.0000
FedAWE [27]	97.16 $\pm$ 0.2792	64.15 $\pm$ 6.8564	33.24 $\pm$ 0.9452
<b>FedAuto (Ours)</b>	<b>98.12</b> $\pm$ 0.1456	<b>75.86</b> $\pm$ 0.8343	<b>50.04</b> $\pm$ 1.8081
FedAvg (Ideal)	97.84 $\pm$ 0.4446	76.54 $\pm$ 1.4070	51.95 $\pm$ 1.6991

of which are vulnerable to connection failures. In the specialized aggregation scheme FedLAW, joint optimization of the introduced shrinking factor and the aggregations weights becomes ineffective when connection failures distort the estimation of client importance, thereby degrading its adaptive aggregation performance. Strategies explicitly designed to handle connection unreliability also face limitations: TF-Aggregation incorporates failure probabilities into the aggregation denominator, which leads to instability under high failure rates. FedAWE increases local stepsizes to compensate for accumulated failure rounds, but becomes ineffective under prolonged connection failures.

**The non-i.i.d. data case.** As shown in Fig. 3(b), 3(d), and 3(f), as well as Table 2, FedAuto consistently maintains stable convergence and high accuracy under non-i.i.d. data, demonstrating strong robustness to both data heterogeneity and connection failures. In contrast, other baselines suffer varying degrees of degradation. Both FedAvg and FedProx, which perform well under i.i.d. data, experience significant drops under non-i.i.d. settings, as prolonged client absence induces biased aggregation toward active clients. These results aligns with the observation (c) of Theorem 1. Besides, TF-Aggregation, SCAFFOLD, FedLAW, and FedAWE all exhibit unstable convergence or suboptimal performance. A closer comparison of Fig. 3(d) and Fig. 3(f) reveals that FedLAW fails to converge on the simpler CIFAR-10 dataset but performs comparatively better on the more complex CIFAR-100 dataset. This behavior stems from the instability of FedLAW’s joint optimization of the shrinking factor and aggregation weights, which relies heavily on client-importance estimation and becomes unreliable under sustained intermittent failures, resulting in task-dependent performance variability.

2) *Partial Client Participation:* We next evaluate FFT strategies under partial client participation with  $K = 10$ , focusing on the most challenging setting that combines mixed connection failures and non-i.i.d. data. Testing accuracies are reported Table 3. Since most FFT strategies exhibit convergence trends under partial participation that are qualitatively similar to those under full participation (Fig. 3), the corresponding convergence curves are provided in Appendix IV-B. As shown in Table 3, FedAuto continues to converge properly and achieves the best testing accuracy across all datasets, with only modest reductions compared to the full-participation results in Table 2. In contrast, several baselines degrade substantially under partial participation. SCAFFOLD suffers severe performance loss, as reduced participation destabilizes the control variate updates in the presence of connection failures. FedLAW also deteriorates markedly, since fluctuating client participation disrupts the optimization of shrinking factors and aggregation weights.

### C. Performance under Partial-Parameter Fine-Tuning (LoRA)

We further evaluate the robustness of FedAuto under the widely adopted partial-parameter fine-tuning strategy, LoRA, on both CIFAR-10 and CIFAR-100 datasets, focusing on the most challenging setting that combines mixed connection failures with non-i.i.d. data. The resulting convergence curves and testing accuracies are reported in Fig. 8 and Table 4.

The results show that FedAuto maintains stable convergence and achieves superior testing accuracy on both datasets. It consistently performs closest to the idealized FedAvg (Ideal), with more pronounced accuracy gains than FFT baselines on the more complex CIFAR-100 dataset. In contrast, on the simpler CIFAR-10 dataset, all FFT baselines that leverage both public and private data underperform Centralized(Public), which trains solely on server-side public data. This indicates that connection failures can disrupt the generalization benefits of pre-trained models, highlighting the fragility of existing FFT baselines under complex and unreliable network conditions.

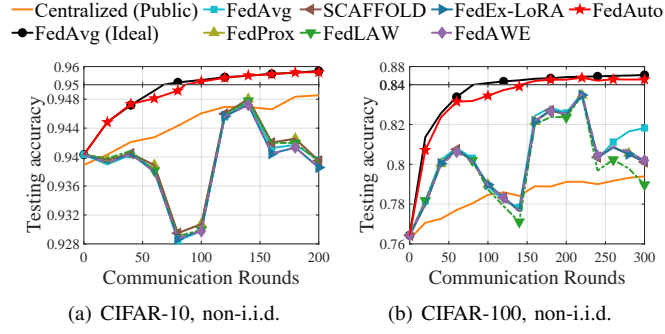


Fig. 4: Convergence trends of different FFT strategies under LoRA ( $K = 20$ , mixed failures).

Table 4: Testing accuracy(%) of different FFT strategies under LoRA ( $K = 20$ , mixed failures, non-i.i.d. data).

FFT Strategy	Dataset	
	CIFAR-10	CIFAR-100
Centralized (Public)	$94.93 \pm 0.1629$	$79.48 \pm 0.6347$
FedAvg [4]	$93.96 \pm 0.4465$	$81.82 \pm 0.6588$
FedProx [22]	$93.95 \pm 0.4426$	$80.14 \pm 1.7574$
SCAFFOLD [23]	$93.95 \pm 0.4426$	$80.12 \pm 1.7358$
FedLAW [33]	$93.94 \pm 0.5050$	$78.97 \pm 2.4693$
FedAWE [27]	$93.85 \pm 0.5453$	$80.20 \pm 1.7281$
FedEx-LoRA [25]	$93.86 \pm 0.5462$	$80.13 \pm 1.7555$
<b>FedAuto (Ours)</b>	<b><math>95.69 \pm 0.1321</math></b>	<b><math>85.15 \pm 0.2928</math></b>
FedAvg (Ideal)	$95.76 \pm 0.1310$	$86.14 \pm 0.2066$

#### D. FedAuto v.s. Resource Allocation Optimization

In this subsection, we compare FedAuto with resource allocation-based baselines to further validate its superiority. Since communication resource optimization can only mitigate transient failures caused by short-term channel fluctuations (e.g., transmission outages in our simulations), but cannot address intermittent failures due to device faults or battery depletion, we consider only transient and mixed failure scenarios involving transient failures. The corresponding results are shown in Fig. 5.

As illustrated in Fig. 5, ResourceOpt-1 exhibits large performance fluctuations. To equalize connection probabilities, it allocates more communication resources to the clients with poor channel conditions and less to those with good conditions, constraining all clients by the worst connections and reducing the number of successfully connected clients per communication round. ResourceOpt-2 achieves suboptimal convergence due to cross-standard differences in connection failure probabilities, leading to imbalanced class contributions during global aggregation. In contrast, FedAuto achieves stable and accurate convergence under different failure modes without requiring network-level resource interventions.

#### E. Ablation Studies

We finally conduct ablation studies to validate the necessity of each module in the adaptive aggregation strategy of FedAuto (Algorithm 2). The experiments are performed under challenging training conditions with mixed failures and non-i.i.d. data, and the results are summarized in Table 5.

1) *Impact of Server-Side Compensation Training:* When server-side compensatory training is disabled, the aggregation weight  $\beta_{\text{miss}}^r$  in (7) is set to zero, and the associated parameters  $\beta_{\text{miss}}^r$  and  $\alpha_{\text{miss},c}^r$  are removed from the optimization problem in (8). Detailed formulations are provided in Appendix III-F. Comparing the first and second rows of Table 5, it is evident that server-side compensatory training markedly improves testing accuracy by mitigating the absence of class-specific local updates caused by unreliable connections. Furthermore, contrasting with third and fourth rows shows that omitting compensatory training from the adaptive aggregation strategy results in significant performance degradation. Although aggregation weight optimization can partially balance the contributions of different data classes, it remains insufficient to compensate for the missing classes, leaving them underrepresented in the global aggregation.

2) *Impact of Aggregation Weight Optimization:* In the absence of aggregation weight optimization, the aggregation weights in (7) reduce to simple averaging. The comparison between the first and third rows of Table 5 demonstrates that aggregation weight optimization improves testing accuracy by better balancing class contributions in the global aggregation. Moreover, comparing the second and fourth rows reveals that while compensatory training alone achieves testing accuracy close to the full strategy on the simpler MNIST dataset, a notable gap remains for the more complex CIFAR-100 dataset. This is because MNIST's simpler feature space allows compensatory training to effectively enhance data diversity and class balance, whereas datasets with richer feature representations require aggregation weight optimization to further balance class contributions and achieve optimal performance.

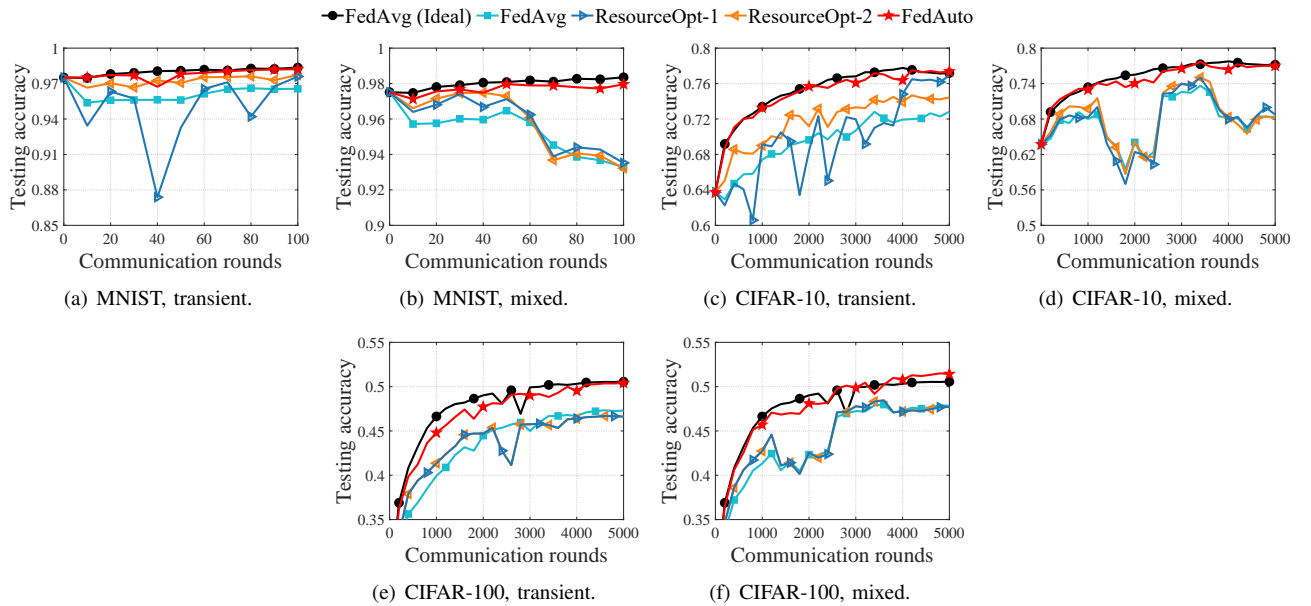


Fig. 5: Convergence trends of FedAuto and resource allocation-based baselines (full-parameter fine-tuning,  $K = 20$ , non-i.i.d.).

Table 5: Testing accuracy (%) of ablation studies ( $K = 20$ , mixed failures, non-i.i.d. data).

Settings		Full-Parameter Fine-Tuning			Partial-Parameter Fine-Tuning (LoRA)		
Server-Side Compensatory Training (Module 1)	Aggregation Weight Optimization (Module 2)	MNIST	CIFAR-10	CIFAR-100	MNIST	CIFAR-10	CIFAR-100
✗	✗	93.28 $\pm$ 1.1806	68.35 $\pm$ 0.3418	47.85 $\pm$ 1.0632	93.87 $\pm$ 0.4356	93.96 $\pm$ 0.4465	81.82 $\pm$ 0.6588
✓	✗	96.68 $\pm$ 0.2654	73.83 $\pm$ 0.5587	49.75 $\pm$ 1.3102	96.15 $\pm$ 0.2168	95.13 $\pm$ 0.2480	83.61 $\pm$ 0.7697
✗	✓	94.06 $\pm$ 1.5616	72.21 $\pm$ 0.7936	47.88 $\pm$ 1.0179	95.10 $\pm$ 0.5654	94.96 $\pm$ 0.3224	82.28 $\pm$ 1.9158
✓	✓	97.96 $\pm$ 0.2489	77.00 $\pm$ 0.5494	51.43 $\pm$ 1.4919	97.06 $\pm$ 0.0750	95.69 $\pm$ 0.1321	85.15 $\pm$ 0.2928

Overall, these results highlight that both server-side compensatory training and aggregation weight optimization are crucial for improving FFT accuracy under unreliable network conditions. They play complementary roles: compensatory training offsets missing classes, while weight optimization ensures balanced contributions across data classes.

## VI. CONCLUSION

This paper investigated the fundamental challenges of FFT in heterogeneous and unreliable network environments, a common yet underexplored setting in practical communication systems. Through theoretical analysis (Theorem 1) and empirical evaluations (e.g., Fig. 2), we showed that the combined effects of connection unreliability and data heterogeneity can severely impair FFT convergence. To address these challenges, we proposed FedAuto, a robust FFT framework that mitigates performance degradation through adaptive aggregation alone. FedAuto requires neither prior knowledge of connection failure statistics nor no modification to existing network infrastructure, enabling seamless plug-and-play deployment in heterogeneous and unreliable networks. We further established a rigorous convergence analysis that provides per-realization convergence guarantees for FedAuto. Extensive experiments on fine-tuning pre-trained models demonstrate that FedAuto consistently outperforms state-of-the-art FFT baselines, underscoring the importance of aggregation-aware design for enhancing practical deployability of FFT. Future work will explore extensions to personalized FL with heterogeneous model architectures, as well as semi-supervised learning under time-varying and class-incremental data distributions.

## REFERENCES

- [1] Y. Wang, Q. Shi, and T.-H. Chang, “Why batch normalization damage federated learning on non-iid data?” *IEEE TNNLS*, pp. 1–15, 2023.
- [2] S. Wang, Y. Xu, Z. Wang, T.-H. Chang, T. Q. Quek, and D. Sun, “Beyond ADMM: A unified client-variance-reduced adaptive federated learning framework,” in *AAAI*, vol. 37, no. 8, 2023, pp. 10 175–10 183.
- [3] S. Wang and T.-H. Chang, “Federated matrix factorization: Algorithm design and application to data clustering,” *IEEE TSP*, vol. 70, pp. 1625–1640, 2022.
- [4] B. McMahan, E. Moore, D. Ramage, S. Hampson, and B. A. y Arcas, “Communication-efficient learning of deep networks from decentralized data,” in *AISTATS*, 2017, pp. 1273–1282.
- [5] J. Zhang, S. Vahidian, M. Kuo, C. Li, R. Zhang, T. Yu, G. Wang, and Y. Chen, “Towards building the FederatedGPT: Federated instruction tuning,” in *IEEE ICASSP*, 2024, pp. 6915–6919.
- [6] W. Kuang, B. Qian, Z. Li, and et al, “Federatedscope-LLM: A comprehensive package for fine-tuning large language models in federated learning,” in *ACM KDD*, 2024, pp. 5260–5271.
- [7] Z. Zhang, Y. Yang, Y. Dai, Q. Wang, Y. Yu, L. Qu, and Z. Xu, “FedPETuning: When federated learning meets the parameter-efficient tuning methods of pre-trained language models,” in *ACL*, 2023, pp. 9963–9977.

[8] L. Zhang, L. Shen, L. Ding, D. Tao, and L.-Y. Duan, "Fine-tuning global model via data-free knowledge distillation for non-iid federated learning," in *IEEE/CVF CVPR*, 2022, pp. 10 174–10 183.

[9] I. Sutskever, "Sequence to sequence learning with neural networks: What a decade," Invited talk at NeurIPS, Vancouver, Canada, 2024.

[10] P. Zheng, Y. Zhu, Y. Hu, Z. Zhang, and A. Schmeink, "Federated learning in heterogeneous networks with unreliable communication," *IEEE TWC*, vol. 23, no. 4, pp. 3823–3838, 2023.

[11] J. Yang, X. Ge, J. Thompson, and H. Gharavi, "Power-consumption outage in beyond fifth generation mobile communication systems," *IEEE TWC*, vol. 20, no. 2, pp. 897–910, 2020.

[12] M. Xiang, S. Ioannidis, E. Yeh, C. Joe-Wong, and L. Su, "Towards bias correction of FedAvg over nonuniform and time-varying communications," in *IEEE CDC*, 2023, pp. 6719–6724.

[13] J. Wang, Q. Liu, H. Liang, G. Joshi, and H. V. Poor, "Tackling the objective inconsistency problem in heterogeneous federated optimization," in *NeurIPS*, vol. 33, 2020, pp. 7611–7623.

[14] M. Mendieta, T. Yang, P. Wang, M. Lee, Z. Ding, and C. Chen, "Local learning matters: Rethinking data heterogeneity in federated learning," in *IEEE/CVF CVPR*, 2022, pp. 8397–8406.

[15] Y. Dai, Z. Chen, J. Li, S. Heinecke, L. Sun, and R. Xu, "Tackling data heterogeneity in federated learning with class prototypes," in *AAAI*, vol. 37, no. 6, 2023, pp. 7314–7322.

[16] M. Chen, Z. Yang, W. Saad, C. Yin, H. V. Poor, and S. Cui, "A joint learning and communications framework for federated learning over wireless networks," *IEEE TWC*, vol. 20, no. 1, pp. 269–283, 2021.

[17] Y. Wang, Y. Xu, Q. Shi, and T.-H. Chang, "Quantized federated learning under transmission delay and outage constraints," *IEEE JSAC*, vol. 40, no. 1, pp. 323–341, 2022.

[18] M. H. Mahmoud, A. Albaseer, M. Abdallah, and N. Al-Dahir, "Federated learning resource optimization and client selection for total energy minimization under outage, latency, and bandwidth constraints with partial or no CSI," *IEEE OJ-COMS*, vol. 4, pp. 936–953, 2023.

[19] M. Ribero, H. Vikalo, and G. De Veciana, "Federated learning under intermittent client availability and time-varying communication constraints," *IEEE JSTSP*, vol. 17, no. 1, pp. 98–111, 2022.

[20] M. Salehi and E. Hossain, "Federated learning in unreliable and resource-constrained cellular wireless networks," *IEEE TC*, vol. 69, no. 8, pp. 5136–5151, 2021.

[21] Y. Wang, W. Ji, J. Zhou, F. Xiao, and T.-H. Chang, "Robust federated learning in unreliable wireless networks: A client selection approach," *IEEE TMC*, pp. 1–18, 2025.

[22] T. Li, A. K. Sahu, M. Zaheer, and et al, "Federated optimization in heterogeneous networks," in *MLSys*, vol. 2, 2020, pp. 429–450.

[23] S. P. Karimireddy, S. Kale, M. Mohri, S. Reddi, S. Stich, and A. T. Suresh, "SCAFFOLD: Stochastic controlled averaging for federated learning," in *ICML*, 2020, pp. 5132–5143.

[24] Z. Wang, Z. Shen, Y. He, G. Sun, H. Wang, L. Lyu, and A. Li, "FLoRA: Federated fine-tuning large language models with heterogeneous low-rank adaptations," in *NeurIPS*, vol. 37, 2024, pp. 22 513–22 533.

[25] R. Singhal, K. Ponkshe, and P. Vepakomma, "FedEx-LoRA: Exact aggregation for federated and efficient fine-tuning of foundation models," *arXiv preprint arXiv:2410.09432*, 2024.

[26] J. Wang, Z. Zhao, Q. Wang, Z. Li, Y. Wang, and T. Q. Quek, "A federated fine-tuning paradigm of foundation models in heterogenous wireless networks," *arXiv preprint arXiv:2509.19306*, 2025.

[27] M. Xiang, S. Ioannidis, E. Yeh, C. Joe-Wong, and L. Su, "Efficient federated learning against heterogeneous and non-stationary client unavailability," in *NeurIPS*, vol. 37, 2024, pp. 104 281–104 328.

[28] A. Z. Tan, H. Yu, L. Cui, and Q. Yang, "Towards personalized federated learning," *IEEE TNNLS*, vol. 34, no. 12, pp. 9587–9603, 2022.

[29] S. Wang, Y. Xu, Y. Yuan, and T. Q. Quek, "Toward fast personalized semi-supervised federated learning in edge networks: Algorithm design and theoretical guarantee," *IEEE TWC*, vol. 23, no. 2, pp. 1170–1183, 2024.

[30] R. A. Bafghi, N. Harilal, C. Monteleoni, and M. Raissi, "Parameter efficient fine-tuning of self-supervised vits without catastrophic forgetting," in *IEEE/CVF CVPR*, 2024, pp. 3679–3684.

[31] E. J. Hu, Y. Shen, P. Wallis, Z. Allen-Zhu, Y. Li, S. Wang, L. Wang, W. Chen et al., "LoRA: Low-rank adaptation of large language models," in *ICLR*, vol. 1, no. 2, 2022.

[32] X. Li, K. Huang, W. Yang, S. Wang, and Z. Zhang, "On the convergence of FedAvg on non-iid data," in *ICLR*, 2020, pp. 1–26.

[33] Z. Li, T. Lin, X. Shang, and C. Wu, "Revisiting weighted aggregation in federated learning with neural networks," in *ICML*, 2023, pp. 19 767–19 788.

[34] M. Grant, S. Boyd, and Y. Ye, "CVX users' guide," 2009.

[35] J. P. Pedroso, "Optimization with gurobi and python," *INESC Porto and Universidade do Porto, Porto, Portugal*, vol. 1, 2011.

[36] J. Ma, X. Sun, W. Xia, X. Wang, X. Chen, and H. Zhu, "Client selection based on label quantity information for federated learning," in *IEEE PIMRC*, 2021, pp. 1–6.

[37] C. Gong, Z. Zheng, Y. Shao, B. Li, F. Wu, and G. Chen, "ODE: An online data selection framework for federated learning with limited storage," *IEEE/ACM ToN*, vol. 32, no. 4, pp. 2794–2809, 2024.

[38] Z. Li, J. Shao, Y. Mao, J. H. Wang, and J. Zhang, "Federated learning with GAN-based data synthesis for non-iid clients," in *FL-IJCAI*, 2022, pp. 17–32.

[39] M. Yang, S. Su, B. Li, and X. Xue, "FedDEO: Description-enhanced one-shot federated learning with diffusion models," in *ACM Multimedia*, pp. 6666–6675.

[40] J. Dong, L. Wang, Z. Fang, G. Sun, S. Xu, X. Wang, and Q. Zhu, "Federated class-incremental learning," in *IEEE/CVF CVPR*, 2022, pp. 10 164–10 173.

[41] J. Dong, H. Li, Y. Cong, G. Sun, Y. Zhang, and L. Van Gool, "No one left behind: Real-world federated class-incremental learning," *IEEE TPAMI*, vol. 46, no. 4, pp. 2054–2070, 2023.

[42] D. C. Nguyen, M. Ding, P. N. Pathirana, A. Seneviratne, J. Li, and H. V. Poor, "Federated learning for internet of things: A comprehensive survey," *IEEE Communications Surveys & Tutorials*, vol. 23, no. 3, pp. 1622–1658, 2021.

[43] X. Wang, W. Chen, J. Xia, Z. Wen, R. Zhu, and T. Schreck, "HetVis: A visual analysis approach for identifying data heterogeneity in horizontal federated learning," *IEEE TVCG*, vol. 29, no. 1, pp. 310–319, 2023.

[44] X. Li, M. JIANG, X. Zhang, M. Kamp, and Q. Dou, "FedBN: Federated learning on non-iid features via local batch normalization," in *ICLR*, 2021.

[45] C. Gong, Z. Zheng, F. Wu, X. Jia, and G. Chen, "Delta: A cloud-assisted data enrichment framework for on-device continual learning," in *MobiCom*, 2024, pp. 1408–1423.

[46] Z. Li, Y. Sun, J. Shao, Y. Mao, J. H. Wang, and J. Zhang, "Feature matching data synthesis for non-iid federated learning," *IEEE TMC*, vol. 23, no. 10, pp. 9352–9367, 2024.

[47] A. Goldsmith, *Wireless communications*. Cambridge University Press, 2005.

[48] A. Correcher, E. García, F. Morant, E. Quiles, and L. Rodríguez, "Intermittent failure dynamics characterization," *IEEE Transactions on Reliability*, vol. 61, no. 3, pp. 649–658, 2012.

[49] Y. LeCun, L. Bottou, Y. Bengio, and P. Haffner, "Gradient-based learning applied to document recognition," *Proceedings of the IEEE*, vol. 86, no. 11, pp. 2278–2324, 1998.

[50] A. Krizhevsky, "Learning multiple layers of features from tiny images," 2009.

[51] K. Hsieh, A. Phanishayee, O. Mutlu, and P. Gibbons, "The non-iid data quagmire of decentralized machine learning," in *ICML*, 2020, pp. 4387–4398.

[52] R. Wightman, "Pytorch image models," <https://github.com/huggingface/pytorch-image-models>, 2019.

- [53] *ETSI EN 301 893 V2.2.1: 5 GHz WAS/RLAN; Harmonised Standard for access to radio spectrum*, European Telecommunications Standards Institute (ETSI) Std., 2024.
- [54] 3rd Generation Partnership Project (3GPP), *3GPP TS 38.101-1 version 15.24.0 Release 15: 5G; NR; User Equipment (UE) radio transmission and reception*, 3GPP Std., 2024.
- [55] *IEEE Standard for Ethernet*, Institute of Electrical and Electronics Engineers (IEEE) Std. IEEE Std 802.3-2018, 2018, clause 25: 100BASE-TX—Physical Layer Specifications.
- [56] C. A. Balanis, *Antenna theory: analysis and design*. John wiley & sons, 2016.

## APPENDIX I PROOF OF REMARK 1

Under reliable network conditions ( $\mathbb{1}_i^r = 1 \forall i, r$ ), global aggregation follows (4). In the case of full participation, where all clients and the server contribute to the aggregation, the aggregation weights are assigned as  $\beta_s^r = p_s$  and  $\beta_i^r = p_i \forall i \in [N]$ . The resulting global model is expressed as

$$\bar{\mathbf{w}}_r = p_s \mathbf{w}_s^{r,E} + \sum_{i=1}^N p_i \mathbf{w}_i^{r,E}, \quad (16)$$

which aligns exactly with the distributed learning objective in (1).

Differently, under partial participation, a subset of  $K$  clients is randomly sampled with replacement from the total  $N$  clients at each round  $r$ . The probability of selecting client  $i \in [N]$  is  $\frac{p_i}{1-p_s}$ . In this setting, the aggregation weight of the server remains  $\beta_s^r = p_s$ , while each selected client  $i \in \mathcal{K}_r$  is assigned a uniform weight  $\beta_i^r = \frac{1-p_s}{K}$ . The aggregated global model is then given by

$$\bar{\mathbf{w}}_r = p_s \mathbf{w}_s^{r,E} + \sum_{i \in \mathcal{K}_r} \frac{1-p_s}{K} \mathbf{w}_i^{r,E}. \quad (17)$$

Because clients are sampled independently according to the defined probability distribution, the expectation of the aggregated global model over the randomness of  $\mathcal{K}_r$  is

$$\mathbb{E}_{\mathcal{K}_r}[\bar{\mathbf{w}}_r] = p_s \mathbf{w}_s^{r,E} + \frac{1-p_s}{K} \sum_{i \in \mathcal{K}_r} \mathbb{E}_{i \in [N]}[\mathbf{w}_i^{r,E}] = p_s \mathbf{w}_s^{r,E} + \frac{1-p_s}{K} \sum_{i \in \mathcal{K}_r} \left( \sum_{i=1}^N \frac{p_i}{1-p_s} \mathbf{w}_i^{r,E} \right) = p_s \mathbf{w}_s^{r,E} + \sum_{i=1}^N p_i \mathbf{w}_i^{r,E}. \quad (18)$$

Thus, the aggregation strategy in (17) yields an unbiased estimate of the global model obtained under full participation, as defined in (16).  $\blacksquare$

## APPENDIX II PROOF OF THEOREM 1

For notational clarity in the subsequent derivations, we unify the indices of the server and clients by introducing  $j \in \{s, [N]\}$ , where  $j = s$  denotes the server and  $j \in [N]$  refers to the clients.

### A. Proof of Convergence Rate

Under Assumption 3, we have

$$F(\bar{\mathbf{w}}_r) \leq F(\bar{\mathbf{w}}_{r-1}) + \langle \nabla F_g(\bar{\mathbf{w}}_{r-1}), \bar{\mathbf{w}}_r - \bar{\mathbf{w}}_{r-1} \rangle + \frac{L}{2} \|\bar{\mathbf{w}}_r - \bar{\mathbf{w}}_{r-1}\|^2. \quad (19)$$

We also need the following three key lemmas, which are proved in subsequent subsections.

**Lemma 1** *Under Assumptions 1, 2 and 3, the following bound holds:*

$$\begin{aligned} & \langle \nabla F_g(\bar{\mathbf{w}}_{r-1}), \bar{\mathbf{w}}_r - \bar{\mathbf{w}}_{r-1} \rangle \\ & \leq -\frac{\gamma E}{2} \sum_{t=1}^E \|\nabla F_g(\bar{\mathbf{w}}_{r-1})\|^2 - \frac{\gamma}{2} \sum_{t=1}^E \left\| \sum_{j \in \{s, [N]\}} \beta_j^r \nabla F_j(\mathbf{w}_j^{r,t-1}) \right\|^2 \\ & \quad + 2\gamma E \chi_{\mathbf{p} \parallel \beta}^2 \sum_{c=1}^C \sum_{j \in \{s, [N]\}} p_j \alpha_{j,c} V_{j,c}^2 + 2\gamma E \chi_{\alpha_g \parallel \tilde{\alpha}^r}^2 G^2 + \gamma L^2 \sum_{j \in \{s, [N]\}} \beta_j^r \sum_{t=1}^E \|\mathbf{w}_j^{r,t-1} - \bar{\mathbf{w}}_{r-1}\|^2, \end{aligned} \quad (20)$$

where  $\chi_{\mathbf{p} \parallel \beta}^2$  and  $\chi_{\alpha_g \parallel \tilde{\alpha}^r}^2$  denote the chi-square divergences defined in (14).

**Lemma 2** *The deviation between the local model at round  $r$  and the global model from the previous round is bounded by*

$$\sum_{t=1}^E \|\mathbf{w}_j^{r,t-1} - \bar{\mathbf{w}}_{r-1}\|^2 \leq \frac{4\gamma^2 E^3}{2 - 3\gamma^2 E^2 L^2} \sum_{c=1}^C (\alpha_{j,c} V_{j,c}^2 + \chi_{\alpha_g \parallel \alpha_j}^2 G^2) + \frac{2\gamma^2 E^3}{2 - 3\gamma^2 E^2 L^2} \|\nabla F_g(\bar{\mathbf{w}}_{r-1})\|^2. \quad (21)$$

**Lemma 3** *Based on the local updating rules in (2) and (3) and the global aggregation rule (4), the difference between the global models at two consecutive rounds satisfies*

$$\bar{\mathbf{w}}_r - \bar{\mathbf{w}}_{r-1} = -\gamma \sum_{j \in \{s, [N]\}} \beta_j^r \sum_{t=1}^E \nabla F_j(\mathbf{w}_j^{r,t-1}), \quad (22)$$

which implies

$$\|\bar{\mathbf{w}}_r - \bar{\mathbf{w}}_{r-1}\|^2 = \gamma^2 \left\| \sum_{t=1}^E \sum_{j \in \{s, [N]\}} \beta_j^r \nabla F_j(\mathbf{w}_j^{r,t-1}) \right\|^2 \stackrel{(a)}{\leq} \gamma^2 E \sum_{t=1}^E \left\| \sum_{j \in \{s, [N]\}} \beta_j^r \nabla F_j(\mathbf{w}_j^{r,t-1}) \right\|^2, \quad (23)$$

where inequality (a) follows from the Cauchy–Schwarz inequality.

Substituting (20) into the second term on the RHS of (19), (23) into the third term, and incorporating (21), we obtain

$$\begin{aligned}
F(\bar{\mathbf{w}}_r) &\leq F(\bar{\mathbf{w}}_{r-1}) - \frac{\gamma E}{2} \|\nabla F_g(\bar{\mathbf{w}}_{r-1})\|^2 - \underbrace{\frac{\gamma(1-\gamma EL)}{2} \sum_{t=1}^E \left\| \sum_{j \in \{s, [N]\}} \beta_j^r \nabla F_j(\mathbf{w}_j^{r,t-1}) \right\|^2}_{(24b)} \\
&\quad + 2\gamma E \chi_{\mathbf{p} \parallel \beta}^2 \sum_{c=1}^C \sum_{j \in \{s, [N]\}} p_j \alpha_{j,c} V_{j,c}^2 + 2\gamma E \chi_{\alpha_g \parallel \tilde{\alpha}^r}^2 G^2 \\
&\quad + \frac{4\gamma^3 E^3 L^2}{2 - 3\gamma^2 E^2 L^2} \sum_{j \in \{s, [N]\}} \beta_j^r \sum_{c=1}^C (\alpha_{j,c} V_{j,c}^2 + \chi_{\alpha_g \parallel \alpha_j}^2 G^2) + \frac{2\gamma^3 E^3 L^2}{2 - 3\gamma^2 E^2 L^2} \|\nabla F_g(\bar{\mathbf{w}}_{r-1})\|^2 \\
&\stackrel{(a)}{\leq} F(\bar{\mathbf{w}}_{r-1}) - \left( \frac{\gamma E}{2} - \frac{2\gamma^3 E^3 L^2}{2 - 3\gamma^2 E^2 L^2} \right) \|\nabla F_g(\bar{\mathbf{w}}_{r-1})\|^2 + 2\gamma E \chi_{\mathbf{p} \parallel \beta}^2 \sum_{c=1}^C \sum_{j \in \{s, [N]\}} p_j \alpha_{j,c} V_{j,c}^2 + 2\gamma E \chi_{\alpha_g \parallel \tilde{\alpha}^r}^2 G^2 \\
&\quad + \frac{4\gamma^3 E^3 L^2}{2 - 3\gamma^2 E^2 L^2} \sum_{j \in \{s, [N]\}} \beta_j^r \sum_{c=1}^C (\alpha_{j,c} V_{j,c}^2 + \chi_{\alpha_g \parallel \alpha_j}^2 G^2), \tag{24}
\end{aligned}$$

where inequality (a) holds by setting  $\gamma EL \leq 1$ , ensuring that (24b)  $\geq 0$ .

Next, summing the above inequality from  $r = 1$  to  $R$  and dividing both sides by  $\gamma T$  (where  $T = RE$  is the total number of local gradient descent steps) yields

$$\begin{aligned}
&\underbrace{\left( \frac{1}{2} - \frac{2\gamma^2 E^2 L^2}{2 - 3\gamma^2 E^2 L^2} \right) \frac{1}{R} \sum_{r=1}^R \|\nabla F_g(\bar{\mathbf{w}}_{r-1})\|^2}_{\triangleq (25a)} \\
&\leq \underbrace{\frac{1}{\gamma T} (F(\bar{\mathbf{w}}_0) - F(\bar{\mathbf{w}}_R))}_{\triangleq (25b)} + \underbrace{\frac{4\gamma^2 E^2 L^2}{2 - 3\gamma^2 E^2 L^2} \frac{1}{R} \sum_{r=1}^R \sum_{j \in \{s, [N]\}} \beta_j^r \sum_{c=1}^C (\alpha_{j,c} V_{j,c}^2 + \chi_{\alpha_g \parallel \alpha_j}^2 G^2)}_{\triangleq (25c)} \\
&\quad + 2\chi_{\mathbf{p} \parallel \beta}^2 \sum_{c=1}^C \sum_{j \in \{s, [N]\}} p_j \alpha_{j,c} V_{j,c}^2 + \frac{2}{R} \sum_{r=1}^R \chi_{\alpha_g \parallel \tilde{\alpha}^r}^2 G^2. \tag{25}
\end{aligned}$$

Let the learning rate be  $\gamma = N^{\frac{1}{2}}/(2LT^{\frac{1}{2}})$  and the number of local updating steps satisfy  $E \leq T^{\frac{1}{4}}/N^{\frac{3}{4}}$ , where  $T \geq N^3$  ensures  $E \geq 1$ . Since  $T \geq 1$  and  $N \geq 1$ , these parameter settings guarantee

$$\gamma EL \leq \frac{1}{2(TN)^{\frac{1}{4}}} \leq \frac{1}{2} < 1, \tag{26}$$

satisfying the condition required for inequality (a) in (24). Moreover, we obtain (25b)  $= 2L/\sqrt{TN}$  and

$$(25c) \leq \frac{\frac{1}{\sqrt{TN}}}{2 - \frac{3}{4\sqrt{TN}}} \stackrel{(a)}{\leq} \frac{\frac{1}{\sqrt{TN}}}{2 - \frac{3}{4}} = \frac{4}{5\sqrt{TN}}, \tag{27a}$$

$$(25a) = \frac{1}{2} - \frac{(25c)}{2} \geq \frac{1}{2} \left( 1 - \frac{4}{5\sqrt{TN}} \right) \geq \frac{1}{2} \left( 1 - \frac{4}{5} \right) = \frac{1}{10}, \tag{27b}$$

where inequality (a) in (27a) is due to  $TN \geq 1$ .

Finally, substituting the above coefficients and  $\bar{\mathbf{w}}_0 = \bar{\mathbf{w}}_{\text{pre}}$  into (25) completes the proof of Theorem 1.  $\blacksquare$

## B. Proof of Lemma 1

From (22), we have

$$\begin{aligned}
&\langle \nabla F_g(\bar{\mathbf{w}}_{r-1}), \bar{\mathbf{w}}_r - \bar{\mathbf{w}}_{r-1} \rangle \\
&= \left\langle \nabla F_g(\bar{\mathbf{w}}_{r-1}), -\gamma \sum_{j \in \{s, [N]\}} \beta_j^r \sum_{t=1}^E \nabla F_j(\mathbf{w}_j^{r,t-1}) \right\rangle \\
&= -\gamma \sum_{t=1}^E \left\langle \nabla F_g(\bar{\mathbf{w}}_{r-1}), \sum_{j \in \{s, [N]\}} \beta_j^r \nabla F_j(\mathbf{w}_j^{r,t-1}) \right\rangle \\
&\stackrel{(a)}{=} -\frac{\gamma}{2} \sum_{t=1}^E \|\nabla F_g(\bar{\mathbf{w}}_{r-1})\|^2 - \frac{\gamma}{2} \sum_{t=1}^E \left\| \sum_{j \in \{s, [N]\}} \beta_j^r \nabla F_j(\mathbf{w}_j^{r,t-1}) \right\|^2 + \frac{\gamma}{2} \sum_{t=1}^E \left\| \nabla F_g(\bar{\mathbf{w}}_{r-1}) - \sum_{j \in \{s, [N]\}} \beta_j^r \nabla F_j(\mathbf{w}_j^{r,t-1}) \right\|^2 \\
&\stackrel{(b)}{\leq} -\frac{\gamma E}{2} \|\nabla F_g(\bar{\mathbf{w}}_{r-1})\|^2 - \frac{\gamma}{2} \sum_{t=1}^E \left\| \sum_{j \in \{s, [N]\}} \beta_j^r \nabla F_j(\mathbf{w}_j^{r,t-1}) \right\|^2 \\
&\quad + \gamma E \left\| \nabla F_g(\bar{\mathbf{w}}_{r-1}) - \sum_{j \in \{s, [N]\}} \beta_j^r \nabla F_j(\bar{\mathbf{w}}_{r-1}) \right\|^2 + \gamma \sum_{t=1}^E \left\| \sum_{j \in \{s, [N]\}} \beta_j^r \nabla F_j(\bar{\mathbf{w}}_{r-1}) - \sum_{j \in \{s, [N]\}} \beta_j^r \nabla F_j(\mathbf{w}_j^{r,t-1}) \right\|^2 \\
&= -\frac{\gamma E}{2} \|\nabla F_g(\bar{\mathbf{w}}_{r-1})\|^2 - \frac{\gamma}{2} \sum_{t=1}^E \left\| \sum_{j \in \{s, [N]\}} \beta_j^r \nabla F_j(\mathbf{w}_j^{r,t-1}) \right\|^2 \\
&\quad + \gamma E \underbrace{\left\| \sum_{j \in \{s, [N]\}} (p_j - \beta_j^r) \nabla F_j(\bar{\mathbf{w}}_{r-1}) \right\|^2}_{\triangleq (28c)} + \gamma \sum_{t=1}^E \underbrace{\left\| \sum_{j \in \{s, [N]\}} \beta_j^r (\nabla F_j(\bar{\mathbf{w}}_{r-1}) - \nabla F_j(\mathbf{w}_j^{r,t-1})) \right\|^2}_{\triangleq (28d)}, \tag{28}
\end{aligned}$$

where equality (a) follows from the identity  $\langle \mathbf{x}_1, \mathbf{x}_2 \rangle = \frac{1}{2}(\|\mathbf{x}_1\|^2 + \|\mathbf{x}_2\|^2 - \|\mathbf{x}_1 - \mathbf{x}_2\|^2)$ , and inequality (b) is derived from the property  $\|\mathbf{x}_1 + \mathbf{x}_2\|^2 \leq 2\|\mathbf{x}_1\|^2 + 2\|\mathbf{x}_2\|^2$ .

In (28), term (28c) can be further bounded as

$$\begin{aligned}
(28c) &\stackrel{(a)}{=} \left\| \sum_{c=1}^C \sum_{j \in \{s, [N]\}} (p_j \alpha_{j,c} - \beta_j^r \alpha_{j,c}) \nabla F_{j,c}(\bar{\mathbf{w}}_{r-1}) \right\|^2 \\
&= \left\| \sum_{c=1}^C \sum_{j \in \{s, [N]\}} (p_j \alpha_{j,c} - \beta_j^r \alpha_{j,c}) \nabla F_{j,c}(\bar{\mathbf{w}}_{r-1}) - \sum_{c=1}^C \sum_{j \in \{s, [N]\}} (p_j \alpha_{j,c} - \beta_j^r \alpha_{j,c}) \nabla F_{g,c}(\bar{\mathbf{w}}_{r-1}) \right. \\
&\quad \left. + \sum_{c=1}^C \sum_{j \in \{s, [N]\}} (p_j \alpha_{j,c} - \beta_j^r \alpha_{j,c}) \nabla F_{g,c}(\bar{\mathbf{w}}_{r-1}) \right\|^2 \\
&\stackrel{(b)}{\leq} 2 \left\| \sum_{c=1}^C \sum_{j \in \{s, [N]\}} (p_j \alpha_{j,c} - \beta_j^r \alpha_{j,c}) (\nabla F_{j,c}(\bar{\mathbf{w}}_{r-1}) - \nabla F_{g,c}(\bar{\mathbf{w}}_{r-1})) \right\|^2 \\
&\quad + 2 \left\| \sum_{c=1}^C \left( \alpha_{g,c} - \sum_{j \in \{s, [N]\}} \beta_j^r \alpha_{j,c} \right) \nabla F_{g,c}(\bar{\mathbf{w}}_{r-1}) \right\|^2 \\
&= 2 \left\| \sum_{c=1}^C \sum_{j \in \{s, [N]\}} \frac{p_j \alpha_{j,c} - \beta_j^r \alpha_{j,c}}{\sqrt{p_j \alpha_{j,c}}} \sqrt{p_j \alpha_{j,c}} (\nabla F_{j,c}(\bar{\mathbf{w}}_{r-1}) - \nabla F_{g,c}(\bar{\mathbf{w}}_{r-1})) \right\|^2 \\
&\quad + 2 \left\| \sum_{c=1}^C \frac{\alpha_{g,c} - \sum_{j \in \{s, [N]\}} \beta_j^r \alpha_{j,c}}{\sqrt{\alpha_{g,c}}} \sqrt{\alpha_{g,c}} \nabla F_{g,c}(\bar{\mathbf{w}}_{r-1}) \right\|^2 \\
&\stackrel{(c)}{\leq} 2 \underbrace{\sum_{c=1}^C \sum_{j \in \{s, [N]\}} \frac{(p_j \alpha_{j,c} - \beta_j^r \alpha_{j,c})^2}{p_j \alpha_{j,c}}}_{\triangleq (29e)} \sum_{c=1}^C \sum_{j \in \{s, [N]\}} p_j \alpha_{j,c} \|\nabla F_{j,c}(\bar{\mathbf{w}}_{r-1}) - F_{g,c}(\bar{\mathbf{w}}_{r-1})\|^2 \\
&\quad + 2 \sum_{c=1}^C \frac{(\alpha_{g,c} - \sum_{j \in \{s, [N]\}} \beta_j^r \alpha_{j,c})^2}{\alpha_{g,c}} \sum_{c=1}^C \alpha_{g,c} \|\nabla F_{g,c}(\bar{\mathbf{w}}_{r-1})\|^2 \\
&\stackrel{(d)}{\leq} 2 \chi_{\mathbf{p} \parallel \boldsymbol{\beta}}^2 \sum_{c=1}^C \sum_{j \in \{s, [N]\}} p_j \alpha_{j,c} V_{j,c}^2 + 2 \chi_{\boldsymbol{\alpha}_g \parallel \boldsymbol{\alpha}^r}^2 G^2, \tag{29}
\end{aligned}$$

where equality (a) follows from (11b), inequality (b) is due to the global class distribution  $\alpha_{g,c} = p_s \alpha_{s,c} + \sum_{i=1}^N p_i \alpha_{i,c}$  together with the inequality  $\|\mathbf{x}_1 + \mathbf{x}_2\|^2 \leq 2\|\mathbf{x}_1\|^2 + 2\|\mathbf{x}_2\|^2$ , and inequality (c) is obtained via the Cauchy–Schwarz inequality. In inequality (c), term (29e) is further bounded as

$$(29e) = \sum_{c=1}^C \sum_{j \in \{s, [N]\}} \frac{(p_j - \beta_j^r)^2 \alpha_{j,c}}{p_j} = \underbrace{\sum_{j \in \{s, [N]\}} \frac{(p_j - \beta_j^r)^2}{p_j}}_{\triangleq \chi_{\mathbf{p} \parallel \boldsymbol{\beta}}^2} \underbrace{\sum_{c=1}^C \alpha_{j,c}}_{=1} = \chi_{\mathbf{p} \parallel \boldsymbol{\beta}}^2. \tag{30}$$

Combining this with Assumptions 1 and 2, as well as the definition of the chi-square divergence  $\chi_{\boldsymbol{\alpha}_g \parallel \boldsymbol{\alpha}^r}^2$  in (14), yields inequality (d) in (29).

Similarly, term (28d) is bounded by

$$(28d) \stackrel{(a)}{\leq} \sum_{j \in \{s, [N]\}} \beta_j^r \|\nabla F_j(\bar{\mathbf{w}}_{r-1}) - F_j(\mathbf{w}_j^{r,t-1})\|^2 \stackrel{(b)}{\leq} L^2 \sum_{j \in \{s, [N]\}} \beta_j^r \|\mathbf{w}_j^{r,t-1} - \bar{\mathbf{w}}_{r-1}\|^2, \tag{31}$$

where inequality (a) follows from Jensen's inequality, and inequality (b) is derived under Assumption 3.

Finally, substituting the bounds obtained in (29) and (31) into (28) establishes Lemma 1.  $\blacksquare$

### C. Proof of Lemma 2

According to the local update rules in (2) and (3), the local model at iteration  $r$  is updated as

$$\mathbf{w}_j^{r,t-1} = \bar{\mathbf{w}}_{r-1} - \gamma \sum_{e=1}^{t-1} \nabla F_j(\mathbf{w}_j^{r,e-1}), \quad j \in \{s, [N]\}. \tag{32}$$

Consequently, the deviation between the local and global models is bounded by

$$\begin{aligned}
&\sum_{t=1}^E \|\mathbf{w}_j^{r,t-1} - \bar{\mathbf{w}}_{r-1}\|^2 \\
&= \sum_{t=1}^E \left\| \gamma \sum_{e=1}^{t-1} \nabla F_j(\mathbf{w}_j^{r,e-1}) \right\|^2 \\
&\stackrel{(a)}{\leq} \gamma^2 \sum_{t=1}^E (t-1) \sum_{e=1}^{t-1} \|\nabla F_j(\mathbf{w}_j^{r,e-1})\|^2 \\
&= \gamma^2 \sum_{t=1}^E (t-1) \sum_{e=1}^{t-1} \|\nabla F_j(\mathbf{w}_j^{r,e-1}) - \nabla F_j(\bar{\mathbf{w}}_{r-1}) + \nabla F_j(\bar{\mathbf{w}}_{r-1}) - \nabla F_g(\bar{\mathbf{w}}_{r-1}) + \nabla F_g(\bar{\mathbf{w}}_{r-1})\|^2 \\
&\stackrel{(b)}{\leq} 3\gamma^2 \sum_{t=1}^E (t-1) \sum_{e=1}^{t-1} \left( \|\nabla F_j(\mathbf{w}_j^{r,e-1}) - \nabla F_j(\bar{\mathbf{w}}_{r-1})\|^2 + \|\nabla F_j(\bar{\mathbf{w}}_{r-1}) - \nabla F_g(\bar{\mathbf{w}}_{r-1})\|^2 + \|\nabla F_g(\bar{\mathbf{w}}_{r-1})\|^2 \right) \\
&\stackrel{(c)}{\leq} 3\gamma^2 L^2 \underbrace{\sum_{t=1}^E (t-1) \sum_{e=1}^{t-1} \|\mathbf{w}_j^{r,e-1} - \bar{\mathbf{w}}_{r-1}\|^2}_{(33d)} + 6\gamma^2 \underbrace{\sum_{t=1}^E (t-1)^2 \sum_{c=1}^C (\alpha_{j,c} V_{j,c}^2 + \chi_{\boldsymbol{\alpha}_g \parallel \boldsymbol{\alpha}_j}^2 G^2)}_{(33e)}
\end{aligned}$$

$$+ 3\gamma^2 \underbrace{\sum_{t=1}^E (t-1)^2 \|\nabla F_g(\bar{\mathbf{w}}_{r-1})\|^2}_{(33e)}, \quad (33)$$

where inequality (a) follows from the Cauchy-Schwarz Inequality, inequality (b) results from  $\|\mathbf{x}_1 + \mathbf{x}_2 + \mathbf{x}_3\|^2 \leq 3\|\mathbf{x}_1\|^2 + 3\|\mathbf{x}_2\|^2 + 3\|\mathbf{x}_3\|^2$ , and inequality (c) holds under Assumptions 3 and Corollary 1.

In (33), the term (33d) is further bounded by

$$\begin{aligned} (33d) &\stackrel{(a)}{=} \sum_{e=1}^{E-1} \left( \sum_{t=e+1}^E t-1 \right) \|\mathbf{w}_j^{r,e-1} - \bar{\mathbf{w}}_{r-1}\|^2 = \sum_{e=1}^{E-1} \left( \sum_{t=e}^{E-1} t \right) \|\mathbf{w}_j^{r,e-1} - \bar{\mathbf{w}}_{r-1}\|^2 \\ &\stackrel{(b)}{=} \sum_{t=1}^{E-1} \left( \sum_{e=t}^{E-1} e \right) \|\mathbf{w}_j^{r,t-1} - \bar{\mathbf{w}}_{r-1}\|^2 \\ &\stackrel{(c)}{\leq} \sum_{t=1}^{E-1} \frac{E^2}{2} \|\mathbf{w}_j^{r,t-1} - \bar{\mathbf{w}}_{r-1}\|^2, \end{aligned} \quad (34)$$

where equality (a) is obtained by interchanging the order of summation, equality (b) follows from re-indexing variables  $e$  and  $t$ , and inequality (c) is derived from  $\sum_{e=t}^{E-1} e = \frac{(t+E-1)(E-1-t+1)}{2} < \frac{(E+t)(E-t)}{2} = \frac{E^2-t^2}{2} < \frac{E^2}{2}$ . Similarly, term (33e) is bounded as

$$(33e) = \sum_{t=1}^E (t-1)^2 = \sum_{t=1}^{E-1} t^2 \stackrel{(a)}{=} \frac{(E-1)E(2E-1)}{6} \leq \frac{E^3}{3}, \quad (35)$$

where equality (a) uses the identity  $\sum_{x=1}^m x^2 = m(m+1)(2m+1)/6$ .

Substituting the bounds from (34) and (35) into (33) gives

$$\begin{aligned} &\sum_{t=1}^E \|\mathbf{w}_j^{r,t-1} - \bar{\mathbf{w}}_{r-1}\|^2 \\ &\leq \frac{3}{2} \gamma^2 E^2 L^2 \sum_{t=1}^E \|\mathbf{w}_j^{r,t-1} - \bar{\mathbf{w}}_{r-1}\|^2 + 2\gamma^2 E^3 \sum_{c=1}^C (\alpha_{j,c} V_{j,c}^2 + \chi_{\alpha_g \mid \alpha_j}^2 G^2) + \gamma^2 E^3 \|\nabla F_g(\bar{\mathbf{w}}_{r-1})\|^2. \end{aligned} \quad (36)$$

Finally, rearranging terms in (36) completes the proof of Lemma 2. ■

### APPENDIX III DETAILED SETTINGS OF EXPERIMENTS

#### A. Network Standards and Communication Resource Allocation

Table 6 summarizes the network standard assigned to each client, along with the corresponding communication resources, including transmit power, bandwidth, and operating frequency band. [53]–[55]

Table 6: Network standard and communication resources allocated to each client.

Standard (Index)	Wired (0)	Wireless			
		Wi-Fi (2.4 GHz) (1)	Wi-Fi (5 GHz) (2)	4G (3)	5G (4)
Client Index	1, 2, 3, 4	5, 9, 13, 17	6, 10, 14, 18	7, 11, 15, 19	8, 12, 16, 20
Transmit Power	-20 dBm (0.01 mW)	20 dBm (100 mW)	23 dBm (200 mW)	23 dBm (200 mW)	23 dBm (200 mW)
Bandwidth	10 MHz	10 MHz	10 MHz	1.8 MHz	2.88 MHz
Frequency Band	Baseband (0)	2.4 GHz	5 GHz	1.8 GHz	3.5 GHz

#### B. Connection Failure Modeling

1) *Transient Failures*: In our setting, wired transmissions are assumed to be stable with negligible loss, whereas wireless transmissions may experience transient failures due to channel fluctuations. For each wireless client, the transient failure probability is derived from a classical path-loss model with shadowing effects [21], [47]. Assuming FDMA for uplink transmission, the channel capacity of each client  $i \in [N]$  in communication round  $r$  is

$$C_i^r = W_i \log_2 \left( 1 + \frac{P_i |h_i^r|^2}{W_i N_0} \right) \text{ bps}, \quad (37)$$

where  $P_i$  and  $W_i$  denote the transmit power and allocated bandwidth (from Table 6), and  $N_0 = -174 \text{ dBm/Hz}$  is the Power Spectrum Density (PSD) of additive noise. The channel gain  $h_i^r$  follows the log-distance path-loss model with shadowing [47]:

$$[|h_i^r|^2]_{\text{dB}} = -[\text{PL}_0(d_0)]_{\text{dB}} - \lambda [d_i]_{\text{dB}} + [\psi_{\text{shadow}}]_{\text{dB}} + [\psi_{\text{wall}}]_{\text{dB}}, \quad (38)$$

where  $\lambda = 3$  is the path-loss exponent,  $d_i$  is the distance to the server, and  $[x]_{\text{dB}}$  denotes the dB representation of  $x$ . Shadowing is modeled as  $[\psi_{\text{shadow}}]_{\text{dB}} \sim \mathcal{N}(0, \sigma_{\text{dB}}^2)$ , with  $\sigma_{\text{dB}} = 4$  for Line of Sight (LOS) and 8 for Non-Line of Sight (NLOS). The wall-loss term is set to 12 dB, 18 dB, 10 dB, and 15 dB per wall under Wi-Fi (2.4 GHz), Wi-Fi (5 GHz), 4G, and 5G, respectively. [54], [55] The free-space reference loss is

$$[\text{PL}_0(d_0)]_{\text{dB}} = 20 \log_{10}(d_i) + 20 \log_{10}(f) + 32.44, \quad (39)$$

where  $d_i$  is in kilometers and  $f$  (MHz) is the carrier frequency from Table 6. [56]

According to the channel coding theorem [47], a transmission outage occurs if the transmission rate  $R_i$  exceeds the instantaneous channel capacity  $C_i^r$ . Thus, the transient failure probability is

$$\epsilon_{i,r}^{\text{TF}} = \Pr(C_i^r \leq R_i), \quad (40)$$

where the transmission rate is given by

$$R_i = \frac{L_i}{\tau_i}, \quad (41)$$

with  $L_i$  denoting the uploaded model size and  $\tau_i$  the transmission delay, specified in Table 7 for each dataset and fine-tuning configuration.

Table 7: Transmission delay for different datasets and fine-tuning configurations.

Parameter	Full-Parameter Fine-Tuning			Partial-Parameter Fine-Tuning		
	MNIST	CIFAR-10	CIFAR-100	MNIST	CIFAR-10	CIFAR-100
<b>Number of Fine-Tuned Parameters</b>	215,466	269,722	11,220,132	302,602	302,602	371,812
Model Size ( $L_i$ )	0.86 M	1.08 M	44.88 M	1.21 M	1.21 M	1.49 M
Transmission Delay per Round ( $\tau_i$ )	0.8 s	1 s	45 s	1.2 s	1.2 s	1.4 s

2) *Intermittent Failures*: Intermittent failures occur randomly and persist for multiple communication rounds. The occurrence of such failures is modeled by an exponential distribution [48], thus the probability that client  $i$  experiences an intermittent failure at round  $r$  is given by

$$\epsilon_{i,r}^{\text{IF}} = 1 - e^{-\lambda_i(r-r_0)}, \quad (42)$$

where  $r_0$  denotes the most recent recovery round, and  $\lambda_i$  is the client-specific failure-rate parameter, as specified in Table 8. Once triggered, the disconnection duration is modeled as a uniform random variable over  $[1, 100/\alpha]$ , where smaller values of  $\alpha$  corresponds to longer interruptions.

Table 8: Intermittent-failure rate of each client.

Client Index	1 – 4	5 – 8	9 – 12	13 – 16	17 – 20
Failure Rate ( $\lambda_i$ )	$10^{-5}$	$10^{-4}$	$10^{-3}$	$10^{-2}$	$10^{-1}$

### C. DNN Architectures for Different Datasets

1) *MNIST*: The small-scale model follows the CNN architecture summarized in Table 9, whereas the large-scale model adopts the ViT architecture specified in Table 10.

Table 9: CNN architecture for MNIST dataset

Layer Name	Output Size	Kernel / Stride	Channels	Normalization	Activation
Conv2d + GroupNorm	28 × 28	5 × 5 / 1	16	GN (4 groups)	ReLU
MaxPool2d	14 × 14	2 × 2 / 2	16	–	–
Conv2d + GroupNorm	14 × 14	5 × 5 / 1	32	GN (4 groups)	ReLU
MaxPool2d	7 × 7	2 × 2 / 2	32	–	–
Flatten	1568	–	–	–	–
Linear	128	–	–	–	ReLU
Linear	10	–	–	–	Softmax

Table 10: ViT architecture for MNIST dataset

Layer Name	Output Size	Kernel / Stride	Channels	Normalization	Activation
Input Image	224 × 224	–	3	–	–
Patch Embedding (Conv2d)	14 × 14 (196 tokens)	16 × 16 / 16	768	–	–
Positional Dropout	196 tokens	–	768	–	–
12 × Transformer Encoder Block (with LoRA)	196 tokens	–	768	LayerNorm	GELU
LayerNorm	196 tokens	–	768	LayerNorm	–
Multi-Head Self-Attention	196 tokens	–	768	–	–
QKV Projection (LoRA, $r=8$ )	196 tokens	–	2304	–	–
Linear Projection	196 tokens	–	768	–	–
LayerNorm	196 tokens	–	768	LayerNorm	–
MLP (FC → GELU → FC)	196 tokens	–	3072 → 768	–	GELU
Final LayerNorm	196 tokens	–	768	LayerNorm	–
Classification Head (Linear)	10	–	–	–	Softmax

2) *CIFAR-10*: The small-scale model uses a ResNet architecture, as shown in Table 11, whereas the large-scale model adopts the same ViT configuration as Table 10.

Table 11: ResNet architecture for CIFAR-10 dataset

Layer Name	Output Size	Kernel / Stride	Channels	Normalization	Activation
Conv2d + GroupNorm	32×32	3×3 / 1	16	GN (4 groups)	ReLU
3 × BasicBlock	32×32	3×3 / 1	16	GN (4 groups)	ReLU
3 × BasicBlock	16×16	3×3 / 2	32	GN (8 groups)	ReLU
3 × BasicBlock	8×8	3×3 / 2	64	GN (16 groups)	ReLU
Global AvgPool	1×1	-	64	-	-
Linear	10	-	-	-	Softmax

3) *CIFAR-100*: The small-scale model employs the ResNet-18 architecture in Table 12, while the large-scale model adopts a ViT architecture similar to that in Table 10, with the output dimension of the final classification head adjusted to 100 to support the 100-class classification task.

Table 12: ResNet-18 architecture for CIFAR-100 dataset

Layer Name	Output Size	Kernel / Stride	Channels	Normalization	Activation
Conv2d + GroupNorm	32×32	3×3 / 1	64	GN (32 groups)	ReLU
2 × BasicBlock	32×32	3×3 / 1	64	GN (32 groups)	ReLU
2 × BasicBlock	16×16	3×3 / 2	128	GN (32 groups)	ReLU
2 × BasicBlock	8×8	3×3 / 2	256	GN (32 groups)	ReLU
2 × BasicBlock	4×4	3×3 / 2	512	GN (32 groups)	ReLU
Global AvgPool	1×1	-	512	-	-
Linear	100	-	-	-	Softmax

#### D. Training Hyperparameters for Fine-Tuning Strategies

The training hyperparameters used for different fine-tuning strategies across all datasets are summarized in Table 13.

Table 13: Training hyperparameters for different datasets and fine-tuning configurations.

Fine-Tuning Strategy	Hyperparameter	Dataset		
		MNIST	CIFAR-10	CIFAR-100
<b>Full-Parameter</b>	<b>Batch Size</b>	128	128	128
	<b>Learning Rate</b>	0.05	0.1 ( $r \leq 4000$ ); 0.01 ( $r > 4000$ )	0.1 ( $r \leq 4000$ ); 0.01 ( $r > 4000$ )
<b>Partial-Parameter (LoRA)</b>	<b>Batch Size</b>	32	32	32
	<b>Learning Rate</b>	0.01	0.01	0.1
	<b>Rank</b>	8	8	8

#### E. Formulations of Baselines

This section summarizes the mathematical formulations of the baselines used in our comparisons, including FL schemes with enhanced aggregation or local training, and FL schemes incorporating communication-resource optimization.

- **FedProx** [22]: This baseline augments each client’s local objective with a proximal regularization term. The local objective becomes

$$F_i(\mathbf{w}) + \frac{\mu}{2} \|\mathbf{w} - \bar{\mathbf{w}}_{r-1}\|^2, \quad (43)$$

where  $\mu$  is the proximal coefficient. For fairness, we report the best performance over  $\mu \in \{0.1, 0.01, 0.001\}$ .

- **SCAFFOLD** [23]: This baseline introduces server- and client-side control variates,  $\mathbf{c}$  and  $\mathbf{c}_i$ , to mitigate data heterogeneity. Each client  $i$  updates its local model and control variate by (44a) and (44b), respectively.

$$\mathbf{w}_i^{r,t} = \mathbf{w}_i^{r,t-1} - \gamma_l (\nabla F_i(\mathbf{w}_i^{r,t-1}) - \mathbf{c}_i + \mathbf{c}), \forall t \in [E], \quad (44a)$$

$$\mathbf{c}_i^+ = \mathbf{c}_i - \mathbf{c} + \frac{1}{K\gamma_l} (\bar{\mathbf{w}}_{r-1} - \mathbf{w}_i^{r,E}). \quad (44b)$$

where  $\gamma_l$  is the local learning rate. The server then updates the global model and the server-side control variates via

$$\bar{\mathbf{w}}_r = \bar{\mathbf{w}}_{r-1} + \frac{\gamma_g}{\sum_{j \in \mathcal{K}_r} \mathbb{1}_j^r} \sum_{i \in \mathcal{K}_r} \mathbb{1}_i^r (\mathbf{w}_i^{r,E} - \bar{\mathbf{w}}_{r-1}), \quad (45a)$$

$$\mathbf{c}^r = \mathbf{c}^{r-1} + \frac{1}{N} \sum_{i \in \mathcal{K}_r} \mathbb{1}_i^r (\mathbf{c}_i^+ - \mathbf{c}_i), \quad (45b)$$

where  $\gamma_g$  is the global learning rate. In our experiments, we set the local learning rate  $\gamma_l = \gamma$ , consistent with the learning rate specified in Table 13, and fix the global learning rate at  $\gamma_g = 1$ .

- **FedLAW** [33]: This baseline leverages a proxy dataset at the server to learn adaptive aggregation weights. Instead of directly averaging local models, the server jointly optimizes a global shrinking factor  $\rho$  and client-specific aggregation weights  $\beta_i$  by solving

$$\rho^*, \beta_i^* = \arg \min_{\rho > 0, \beta_i \geq 0} \mathcal{L}_{\text{proxy}} \left( \rho \sum_{i \in \mathcal{K}_r} \beta_i \mathbf{w}_i^{r,E} \right), \quad (46)$$

where  $\mathcal{L}_{\text{proxy}}$  denotes the empirical loss evaluated on the proxy dataset. The optimized parameters are then used to update the global model as

$$\bar{\mathbf{w}}_r = \rho^* \sum_{i \in \mathcal{K}_r} \beta_i^* \mathbf{w}_i^{r,E}. \quad (47)$$

- **TF-Aggregation** [20]: This baseline incorporates the transient connection failure probability into the denominator of the global aggregation. Specifically, the global aggregation in Step 9 of Algorithm 1 is modified as

$$\bar{\mathbf{w}}_r = \frac{1}{K} \sum_{i \in \mathcal{K}_r} \mathbf{1}_i^r \frac{p_i}{s_i(1 - \epsilon_i)} \mathbf{w}_i^{r,E}, \quad (48)$$

where  $\epsilon_i$  denotes the connection failure probability of client  $i$ , and client selection probabilities  $\{s_i\}$  are optimized by

$$\min_{s_i} \sum_{i=1}^N \frac{p_i}{s_i(1 - \epsilon_i)}, \quad (49a)$$

$$\text{s.t. } s_i \geq 0, \forall i \in [N]; \sum_{i=1}^N s_i = 1. \quad (49b)$$

To avoid inefficient selection when  $\epsilon_i \rightarrow 1$ , clients with excessively high failure probabilities are excluded via a reliability threshold  $\epsilon_{\text{th}}$ . The optimization problem in (49) is then modified as

$$\min_{s_i} \sum_{i=1, \epsilon_i^0 \leq \epsilon_{\text{th}}}^N \frac{p_i}{s_i(1 - \epsilon_i^0)}, \quad (50a)$$

$$\text{s.t. } s_i \geq 0 \text{ if } \epsilon_i^0 \leq \epsilon_{\text{th}}; s_i = 0 \text{ if } \epsilon_i^0 > \epsilon_{\text{th}}, \quad (50b)$$

$$\sum_{i=1, \epsilon_i^0 \leq \epsilon_{\text{th}}}^N s_i = 1. \quad (50c)$$

where the initial transient failure probability  $\epsilon_i^0$  is computed according to the formulations in Appendix III-B, and the threshold is set to  $\epsilon_{\text{th}} = 0.9$  in our experiments.

- **FedAWE** [27]: This baseline adapts each client's local update according to its history of successful connections. After performing the  $E$ -step local update in (2), client  $i$  further adjusts its local model  $\mathbf{w}_i^{r,E}$  as

$$\mathbf{w}_i^{r,E} = \mathbf{w}_i^{r,E} - \gamma_g(r - \tau_i)(\bar{\mathbf{w}}_{r-1} - \mathbf{w}_i^{r,E}), \quad (51)$$

where  $\gamma_g$  denotes the global learning rate (set to 0.001), and  $\tau_i$  is the most recent round in which client  $i$  successfully connected to the server. If client  $i$  connects in every round, then  $\tau_i = r - 1$ .

- **FedEx-LoRA** [25]: This baseline incorporates an error-residual correction induced by the global aggregation of LoRA modules into local updates. Given a pretrained model  $\mathbf{w}_{\text{pre}}$  fine-tuned via low-rank adapters  $\mathbf{A}$  and  $\mathbf{B}$ , the server aggregates client adapters at round  $r$  following FedAvg:

$$\bar{\mathbf{B}}^r = \frac{1}{\sum_{j \in \mathcal{K}_r} \mathbf{1}_j^r} \sum_{i \in \mathcal{K}_r} \mathbf{1}_i^r \mathbf{B}_i^{r,E}, \quad \bar{\mathbf{A}}^r = \frac{1}{\sum_{j \in \mathcal{K}_r} \mathbf{1}_j^r} \sum_{i \in \mathcal{K}_r} \mathbf{1}_i^r \mathbf{A}_i^{r,E}. \quad (52)$$

The induced error-residual is computed as

$$\Delta \mathbf{w}_{\text{res}}^r = \left( \frac{1}{\sum_{j \in \mathcal{K}_r} \mathbf{1}_j^r} \sum_{i \in \mathcal{K}_r} \mathbf{1}_i^r \mathbf{B}_i^{r,E} \mathbf{A}_i^{r,E} \right) - \bar{\mathbf{B}}^r \times \bar{\mathbf{A}}^r. \quad (53)$$

Clients update the pretrained model as  $\mathbf{w}_{\text{pre}}^r = \mathbf{w}_{\text{pre}}^r + \Delta \mathbf{w}_{\text{res}}^r$ , and initialize the next-round adapters as  $\mathbf{B}_i^{r+1,0} = \bar{\mathbf{B}}^r$  and  $\mathbf{A}_i^{r+1,0} = \bar{\mathbf{A}}^r$ .

- **ResourceOpt-1**: Motivated by [17, Corollary 1], this baseline seeks to reduce convergence bias by equalizing clients' transient connection failure probabilities. To this end, the optimization problem in (54) jointly allocates each client's transmit power  $P_i$  and bandwidth  $W_i$  to minimize the variance of their failure probabilities.

$$\min_{P_i, W_i, i \in [N]} \frac{1}{2} \sum_{i \in [N], \epsilon_i^0 \leq \epsilon_{\text{th}}} \left\| \epsilon_i - \underbrace{\frac{\sum_{i \in [N], \epsilon_i^0 \leq \epsilon_{\text{th}}} \epsilon_i}{\sum_{i \in [N], \epsilon_i^0 \leq \epsilon_{\text{th}}} 1}}_{\triangleq \bar{\epsilon}} \right\|^2, \quad (54a)$$

$$\text{s.t. } P_i \leq P_s^{\max}, \forall i \in [N] \text{ and } \epsilon_i^0 \leq \epsilon_{\text{th}}, \quad (54b)$$

$$\sum_{i \in \mathcal{S}_s} W_i \leq W_s^{\text{total}}, \forall i \in [N] \text{ and } \epsilon_i^0 \leq \epsilon_{\text{th}}. \quad (54c)$$

In (54a),  $\epsilon_i$  denotes the transient failure probability of client  $i$ , and  $\bar{\epsilon}$  is the corresponding average across all eligible clients. We impose  $\epsilon_i^0 \leq \epsilon_{\text{th}} = 0.9$  to avoid selecting highly unreliable clients, consistent with the TF-Aggregation baseline. Constraints (54b)-(54c) limit each client's transmit power and bandwidth based on the maximum allowable values  $P_s^{\max}$  and  $W_s^{\text{total}}$ , respectively, where  $s \in \{0, 1, 2, 3, 4\}$  corresponds to the communication standards in Table 6 and  $\mathcal{S}_s$  denotes the set of clients operating under standard  $s$ . Since wired clients ( $s = 0$ ) exhibit negligible failure probability, we refine (54) into the modified formulation (55). This formulation first optimizes wireless clients ( $s = 1-4$ ) under (55a)-(55c), then enforces (55d) by aligning wired clients' failure probabilities to  $\bar{\epsilon}$  via random dropping of received models at the server:

$$\min_{P_i, W_i, \{\mathcal{S}_s\}_{s=1}^4} \frac{1}{2} \sum_{i \in \{\mathcal{S}_s\}_{s=1}^4, \epsilon_i^0 \leq \epsilon_{\text{th}}} \left\| \epsilon_i - \underbrace{\frac{\sum_{i \in [N], \epsilon_i^0 \leq \epsilon_{\text{th}}} \epsilon_i}{\sum_{i \in [N], \epsilon_i^0 \leq \epsilon_{\text{th}}} 1}}_{\triangleq \bar{\epsilon}} \right\|^2, \quad (55a)$$

$$\text{s.t. } P_i \leq P_s^{\max}, \forall i \in \{\mathcal{S}_s\}_{s=1}^4 \text{ and } \epsilon_i^0 \leq \epsilon_{\text{th}}, \quad (55b)$$

$$\sum_{i \in \mathcal{S}_s} W_i \leq W_s^{\text{total}}, \forall i \in \{\mathcal{S}_s\}_{s=1}^4 \text{ and } \epsilon_i^0 \leq \epsilon_{\text{th}}, \quad (55c)$$

$$\epsilon_i = \bar{\epsilon}, \forall i \in \mathcal{S}_0. \quad (55d)$$

Given the smooth and continuous gradients of (55a) due to the squared terms, we apply gradient descent to optimize the transmit power  $P_i$  and bandwidth  $W_i$  for clients satisfying  $\epsilon_i^0 \leq \epsilon_{\text{th}}$ .

- **ResourceOpt-2:** Because joint resource optimization across heterogeneous communication standards is often impractical in real-world deployments, this baseline performs standard-wise optimization. For each standard  $s \in \{0, 1, 2, 3, 4\}$ , the following problem is solved independently:

$$\min_{P_i, W_i, \substack{i \in \mathcal{S}_s \\ \epsilon_i^0 \leq \epsilon_{\text{th}}}} \frac{1}{2} \sum_{i \in \mathcal{S}_s, \epsilon_i^0 \leq \epsilon_{\text{th}}} \left\| \epsilon_i - \frac{\sum_{i \in \mathcal{S}_s, \epsilon_i^0 \leq \epsilon_{\text{th}}} \epsilon_i}{\sum_{i \in \mathcal{S}_s, \epsilon_i^0 \leq \epsilon_{\text{th}}} 1} \right\|^2, \quad (56a)$$

$$\text{s.t. } P_i \leq P_s^{\max}, \forall i \in \mathcal{S}_s \text{ and } \epsilon_i^0 \leq \epsilon_{\text{th}}, \quad (56b)$$

$$\sum_{i \in \mathcal{S}_s} W_i \leq W_s^{\text{total}}, \forall i \in \mathcal{S}_s \text{ and } \epsilon_i^0 \leq \epsilon_{\text{th}}. \quad (56c)$$

#### F. Formulations for Ablation Studies

1) *Without Server-Side Compensation Training:* When the server-side compensatory training module is disabled, the global aggregation rule in (7) reduces to (5). Consequently, the aggregation weight optimization problem (8) simplifies to

$$\min_{\beta_s^r, \{\beta_i^r\}_{i=1}^r} \sum_{c=1}^C \frac{\left( \alpha_{g,c} - (\beta_s^r \alpha_{s,c} + \sum_{i \in \mathcal{K}_r} \mathbf{1}_i^r \beta_i^r \alpha_{i,c}) \right)^2}{\alpha_{g,c}}, \quad (57a)$$

$$\text{s.t. } \beta_s^r + \sum_{i \in \mathcal{K}_r} \mathbf{1}_i^r \beta_i^r = 1. \quad (57b)$$

Analogous to (8), the formulation in (57) remains a convex weighted least squares problem and can be easily solved by standard quadratic optimization solvers. Following the procedure in Section III-B, the server-side aggregation weight continues to be fixed as (9).

2) *Without Aggregation Weight Optimization:* When aggregation weight optimization is removed, the global aggregation rule in (7) degenerates into a simple averaging scheme. In this case, while the server weight remains fixed as (9), all remaining aggregation weights, including  $\beta_{\text{miss}}^r$  and  $\beta_i^r$ , are assigned by simple averaging:

$$\begin{cases} \beta_{\text{miss}}^r = 0, \quad \beta_i^r = \frac{1}{1 + \sum_{j \in \mathcal{K}_r} \mathbf{1}_j^r}, & \text{if } \mathcal{C}_{\text{miss}}^r = \emptyset, \\ \beta_{\text{miss}}^r = \beta_i^r = \frac{\sum_{j \in \mathcal{K}_r} \mathbf{1}_j^r}{(1 + \sum_{j \in \mathcal{K}_r} \mathbf{1}_j^r)^2}, & \text{if } \mathcal{C}_{\text{miss}}^r \neq \emptyset. \end{cases} \quad (58)$$

Under these assignments, all aggregation weights continue to satisfy the normalization constraint in (8b).

## APPENDIX IV SUPPLEMENTARY EXPERIMENTAL RESULTS

### A. Convergence Trends under Transient and Intermittent Failures

Fig. 6 illustrates the convergence trends of different FFT strategies under transient connection failures across MNIST, CIFAR-10, and CIFAR-100 for both i.i.d. and non-i.i.d. data settings. Fig. 7 presents the corresponding results under intermittent failures.

### B. Convergence Trends under Partial Participation

Fig. 8 compares the convergence trends of different FFT strategies under partial participation.

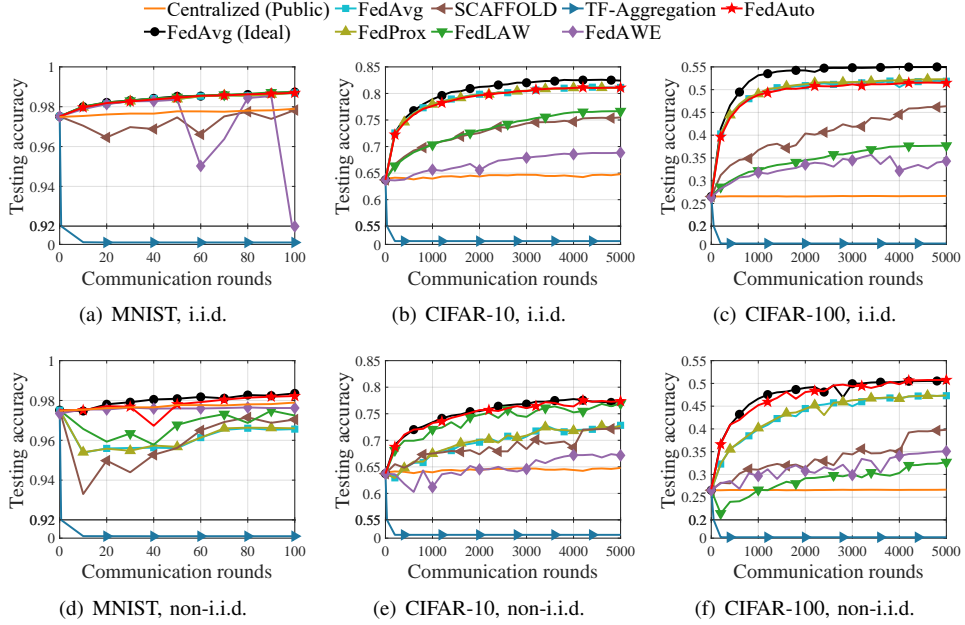


Fig. 6: Convergence trends of different FFT strategies under transient failures ( $K = 20$ , full-parameter fine-tuning).

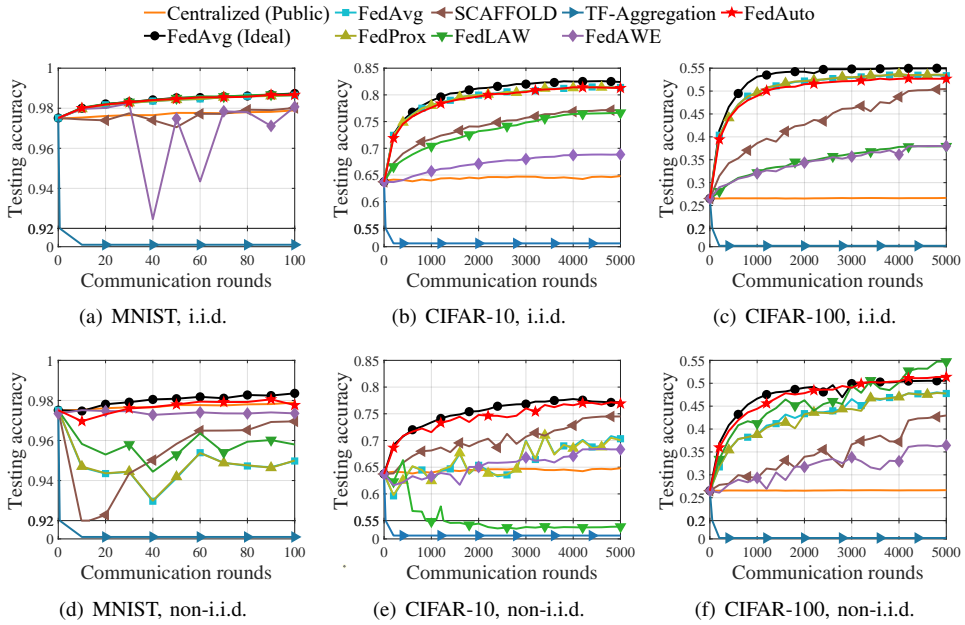


Fig. 7: Convergence trends of different FFT strategies under intermittent failures ( $K = 20$ , full-parameter fine-tuning).

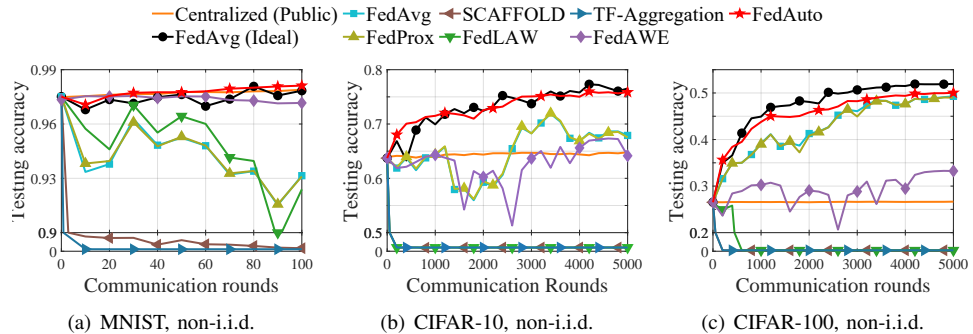


Fig. 8: Convergence of different FFT strategies under full-parameter fine-tuning with partial participation ( $K = 10$ , mixed failures).